Simulating biotechnological processes affected by meteorology: Application to algae–bacteria systems

Francesca Casagli, Olivier Bernard

Simulating biotechnological processes affected by meteorology: application to algae-bacteria systems

Francesca Casagli[a], Olivier Bernard[a,b*]

[a]*BIOCORE, INRIA, Université côte d'Azur, BP 93, 06902 Sophia-Antipolis Cedex, France.*
[b]*LOV, Sorbonne University, CNRS, UMR 7093, Station Zoologique, BP 28, 06234 Villefrance-sur-mer, France.*

Abstract

Most of the existing mathematical models for outdoor biotechnological processes require the measurement of the medium temperature, and therefore, they cannot forecast the process dynamics in the future or perform scenario analysis under different climatology. Fully predictive models are thus required for advanced predictions and optimization of environmental bioprocesses affected by weather fluctuations. This is of major importance for supporting the industries in the bioprocess design, decision making and process management.

Here, we introduce the FLAME modelling framework for forecasting the fate of outdoor bioprocesses. It integrates, on top of a biological model conserving carbon, nitrogen and phosphorus, a heat transfer model and a chemical sub-model for computing the speciation of all the dissociated chemical molecules. The versatile FLAME modelling platform includes different modules with balanced complexities. Alternative biological models can eas-

*Corresponding author
Email address: olivier.bernard@inria.fr (Olivier Bernard[a,b*])

ily be interchanged, in order to promote a dialog for bioremediation model comparisons and improvements.

The approach is illustrated with an algae-bacteria wastewater treatment pond, subjected to the solar flux and to the meteorological events (wind, rain, ...). The fully predictive model was validated over more than one year, therefore representing all the seasons. The temperature prediction turns out to be crucial, especially to appropriately simulate nitrification. The model estimates the dynamics of the different biomasses in the system, providing a diagnosis tool to follow the hidden part of the process dynamics. The proposed framework is a powerful tool for advanced control and optimization of environmental processes, which can guide the scaling up and management of the most innovative bioprocesses.

Keywords: Algae-bacteria, temperature, meteorology, chemical model, modelling framework, wastewater

---

Nomenclature

ADM1	Anaerobic Digestion Model 1
ALBA	ALgae-BActeria model
AOB	Ammonium Oxidizing Bacteria
ASMx	Activated Slude Model x
BSM2	Benchmark Simulation Model no. 2
COD	Chemical Oxygen Demand
FLAME	Framework for physicaL-biologicAl ModEls
HRT	Hydraulic Retention Time
HRABP	High Rate Algae Bacteria Pond
IWA	International Water Association
MPC	Model Predictive Control
NOB	Nitrite Oxidizing Bacteria
PAR	Phosynthetic Active Radiation
PDE	partial differential equations
SRT	Solid Retention Time
TA	Total Alkalinity
TSS	Total Suspended Solids
VFA	Volatile Fatty Acids
VSS	Volatile Suspended Solids
WWTP	WasteWater Treatment plant

1. Introduction

Modelling environmental biotechnological processes is a challenging task which requires long term experimental and mathematical developments (Dochain and Vanrolleghem, 2001; Osborne et al., 2014; Mairet and Bernard, 2019). So far, most of the modelling efforts have been focused on the identification of reliable biological models balancing the mathematical and the underlying ecological complexity by appropriately choosing the number of involved species and processes. A new generation of models of increasing complexity is now appearing (see Table. 1) based on elemental conservation, in the perspective of developing more efficient processes for recycling energy, nitrogen and phosphorus. These environmental outdoor processes are deeply affected by the climate which triggers the medium temperature (Zouboulis and Tolkou, 2015; Plósz et al., 2009) and thus the biological activities. Including the effect of temperature in the associated numerical models did so far not receive the requested attention and this paper focuses on this challenge.

Activated sludge plants are known to be directly influenced by the weather (Luo et al., 2020). Operating them in winter is typically more complicated than in summer due to the slower kinetics. The impact of meteorology is marked even for anaerobic digesters which generally have a temperature regulation system. Yu et al. (2021) showed that inefficient temperature regulation due to weather fluctuations can lead to a loss of methane production by 20%. Temperature probably impacts even more strongly the emerging algae/bacteria systems for wastewater remediation. These processes are seen

as a key player to enhance wastewater treatment by producing the oxygen through photosynthesis, avoiding therefore the expensive cost of aeration (Rossi et al., 2020b). In addition, the algal biomass has a valuable potential to be used as byproduct (e.g. biofuels, biofertilizer and bioplastics), matching a circular economy approach. Algae/bacteria are grown together in shallow (typically less than 0.3 m) outdoor raceways, strongly depending on the solar flux for photosynthesis (Milledge, 2011). Being shallow, these systems have a low thermal inertia and temperature can very rapidly change in response to meteorology, eventually leading to large variations in the medium temperature (Béchet et al., 2011).

Better representing wastewater treatment processes have motivated two decades of model development with the objective of supporting advanced process supervision and optimization. The first models emerged for activated sludge (ASM1,ASM3,(Henze et al., 2000a)) and anaerobic digestion (ADM1, (Batstone et al., 2002)). A long list of variant models have been developed (Janus and Ulanicki, 2010; Barrera et al., 2015; Buaisha et al., 2020) including also models for the algae-bacteria processes (Broekhuizen et al., 2012; Solimeno et al., 2019; Casagli et al., 2021b). A list of the most widespread models for environmental processes can be found in Table 1.

Looking closer to these models, it turns out that they cannot be used for forcasting, since they require medium temperature measurements, which evolves, depending on the meteorology. Paradoxically, we are now in a situation where these models are not able to meet one of the key objective for

which they were designed: optimization of outdoor industrial processes. This missing step for full predictions is somehow critic since most of the environmental processes are permanently submitted to temperature variations due to the nonstationarity of the solar flux combined with meteorology.

Predicting the dynamics of these processes needs first to get reliable weather forecasts, at least for the short term and, second, a heat transfer model for forecasting the reactor temperature dynamics. Forecasting temperature in an outdoor process is not challenging in itself, and several thermal models are available in the literature (la Cour Jansen et al., 1992; Sedory and Stenstrom, 1995; Lippi et al., 2009). Nevertheless, integrated models predicting at the same time medium temperature and biological activity are still very rare, as well as their long-term validation.

This results from several bottlenecks, that together prevented the development of fully predictive models. The first challenge is to coherently manage the climatological information (solar flux, air temperature, wind velocity,...) in the different submodels (heat transfer model, chemical model, biological model). As a matter of illustration, the solar flux must be considered both in the heat transfer model (solar irradiance at the ground level, in W m^{-2}) and in the processes involving photosynthesis (Photosynthetically Active Radiation, PAR, in μ mol m^{-2} s^{-1}). The second challenge is to balance the model complexity and its accuracy (Mairet and Bernard, 2019), with a similar treatment for all the submodels. The accuracy of the biological model should be similar to the one of the heat transfer model. Then, the same simulation

platform must be used for the two submodel, to automatically run the fully predictive model embedding the set of interconnected submodels. Most of the heat transfer models are run from computational fluid dynamics frameworks, often requiring a human intervention. This prevent any automatic use of the model for on-line control purpose. Finally, the precise way temperature affects the enzymatic reactions governing microbial life and more generally the growth rate of the involved organisms must have been well represented in the biological kinetics and accurately calibrated. Temperature also affects the speciation of the chemical compounds and their availability in the medium, and this temperature dependence must be implemented in the model.

None of these issues taken separately represents a critical difficulty, but the complexity of their combination probably explains the present lack of fully predictive models.

The objective of this paper is to introduce the FLAME (Framework for physicaL-biologicAl ModEls) framework, specifically developed for linking the mass (C, N and P) and energy fluxes within the biological, physical and chemical modules. The proposed approach leads to a framework where full predictions become possible. This is the cornerstone for advanced monitoring, design and control strategies opening the door to optimization of the process efficiency, with simultaneous reduction of environmental impacts (Klemeš et al., 2012; Yong et al., 2016; Van Fan et al., 2018, 2020).

The proposed approach is generic and can be applied to several out-

Table 1: Examples of models for WWT processes which could benefit from the FLAME modules. Green ticks point out the model implementation already done according to the proposed FLAME framework. Black ticks point out the FLAME modules that can be implemented. Red ticks point out the expected upgrading when using the FLAME framework, according to the current limitation: [1] Only monoprotic acids and/or limited amount of chemicals considered; [2] No evaporation; [3] Only O_2 stripping/dissolution considered (no CO_2 and NH_3).

WWT Process	Biological models (reference)	FLAME chemical	FLAME heat	FLAME I/O
Algae/Bacteria	**ALBA** Casagli et al. (2021b)	✓	✓	✓
	BIOALGAE2 Solimeno et al. (2019)	✓[1]	✓	✓[2]
	ABACO Sánchez-Zurano et al. (2021)	✓	✓	✓
	Modified ASM3 Arashiro et al. (2017)	✓	✓	✓
	Modified RWQM1 Broekhuizen et al. (2012)	✓[1]	✓	✓[2,3]
	PHOBIA Wolf et al. (2007)	✓	✓	✓
	ASMA Wágner et al. (2016)	✓	✓	✓
Activated sludge	**ASM1, ASM2, ASM2d, ASM3** Henze et al. (2000b)	✓	✓	✓[2,3]
Anaerobic digestion	**ADM1** Batstone et al. (2002)	✓[1]	✓	..

door bioprocesses, but it is detailed and illustrated for the specific case of algae-bacteria systems. The high-fidelity biological ALBA (ALgae BActeria) model is used here for sake of illustration. It can be interchanged with other biological models to include a different description of the process. The FLAME framework is progressively described along the paper and its theory is illustrated point by point with algae-bacteria outdoor systems.

First, we present a brief review of existing heat transfer models which

have been developed for environmental bioprocesses. The following paragraph details the material and methods used along the paper. We provide a detailed description of the experimental data which were used to validate the case study. Information on the model implementation are also provided. In section 4 we introduce the FLAME framework, and the structure of the general model. We detail and illustrate the different compartments using the algae-bacteria process as example of application. We propose an effective heat transfer model, and a general approach to represent chemical equilibria in the process. Finally we provide details about the different fluxes from and towards the environment. In section 5 we validate our approach with data from a campaign (Casagli et al., 2021b) on an algae-bacteria process. The fully predictive model turns out to be very accurate, even for winter periods. The model highlights the difference in the microbial community between the cold and the hot seasons. We show that temperature indirectly impacts alkalinity, with a strong influence on the dynamics of ammoniacal nitrogen removal.

2. Review of full predictive models for environmental biotechnological processes

The pioneer heat transfer model of la Cour Jansen et al. (1992) was developed for an activate sludge process and validated along a full year with data from a plant in Denmark. Later, another heat transfer model was developed for an aeration tank by Sedory and Stenstrom (1995) and validated

in July and January across WWTP in the US. It turned out that predicting temperature in winter was more challenging. This model was later improved by Lippi et al. (2009). The model of Makinia et al. (2005) for activated sludge tank was validated along the year in a WWTP in Oregon. Once again the critical winter period was the less accurately represented. More recently, Arnell et al. (2021) explicitly coupled a heat transfer model to the BSM2 modelling framework with different tanks in a WWTP in Sweeden and validated the temperature model along the year.

All these models are based on dynamical temperature simulations, resulting from a first order model. The temperature influence on biological kinetics in the most advanced cases is implemented with the Arrhenius law. Moreover, the fluxes of C, N and P are not represented, and therefore, only a simplified chemical model is typically implemented.

The temperature effect is more systematically included in the modelling works dealing with microalgae based processes (Broekhuizen et al., 2012; Solimeno et al., 2019; Casagli et al., 2021b). Indeed, solar radiation is key for photosynthesis, and associated with the solar heat flux. However, for all these models, temperature was assumed to be experimentally measured, which definitely hinders the prediction capability of bioprocess models. The model of Béchet et al. (2011) was previously developed for predicting the temperature in raceway ponds producing microalgae. However, its implementation requires to integrate a partial differential equation (PDE) describing temperature in the ground, to determine the conductivity term. Such

computational complexity lead some authors to measure the ground temperature in order to run the model (Rodríguez-Miranda et al., 2021). However this solution jeopardizes any attempt to assess various operating strategies or process implementation at a different location. A heat transfer model, extending the one of Béchet et al. (2011), is proposed here, replacing the PDE by the temperature dynamics of the material enveloping the water mass, which is partially in contact with the ground. Finally it leads to a differential equation of dimension 2 which is embedded in the FLAME framework.

3. Materials and Methods

3.1. Pilot raceway application for validating the fully predictive ALBA model

The experiments were carried out with an outdoor High Rate Algae Bacteria Pond (HRABP) located at INRAE, Narbonne, southern France (Latitude: 43.15656, Longitude: 2.994438), with a total surface area of 56 m^2 and a channel length of 15 m (see Figure 1).

The raceway was operated in continuous mode, from 15/05/2018 to 01/08/2019. The influent flow rate was set to obtain a Hydraulic Retention Time (HRT) of 5 days along the whole experimental period, except from one month (29/08/2018-29/09/2018) during which different HRT values (ranging from 2 to 10 days) were tested. The HRABP was also equipped with online dissolved oxygen, temperature, pH and incident PAR probes. Off-line measurements of Total Suspended Solids, Chemical Oxygen Demand (total and soluble), ammonium, nitrate and nitrite were carried out. The air temperature, wind

Figure 1: High Rate Algae-Bacteria pond (HRABP) located in Narbonne (F).

speed and relative humidity data, necessary for determining the pond temperature through the model, were acquired from the nearest weather station (Béziers, France, Latitude: 43.3235, Longitude: 3.3539), located at approximately 30 km from the pond. The local rainfall rate was recorded on-site. Additional information on the experimental protocol can be found in Casagli et al. (2021b), and they are also summarized in Appendix A.

3.2. Model implementation

To guaranty the accuracy in the implementation of this complex model, it was independently implemented in Aquasim (Reichert, 1994) and Matlab R2019a. Removing buggs and ensuring a safe model code is crucial, and a double implementation guarantees the model soundness (Mairet and Bernard, 2019). The numerical integration under Matlab was carried out

with the ode15s variable-step, variable-order solver based on the numerical differentiation formulas of orders 1 to 5 (Shampine et al., 1999). The relative tolerance was set to 10^{-6}. Such solver for stiff Ordinary Differential Equations (ODE) is necessary to well manage the integration with the pH sub-model, running at a faster time scale. In Aquasim, the ODE (biological and heat transfer) and the algebraic equations (chemical equilibria) are integrated according to the DASSL algorithm (Petzold, 1982; Reichert, 1998).

4. General FLAME modelling framework

4.1. General structure

The general predictive model structure results from the three following key components:

1. A submodel for the heat transfer to predict the medium temperature from solar flux, wind, air temperature and relative humidity.
2. A submodel representing the chemical processes, including the ionic balances, the dissociation constants and their temperature dependence.
3. A model representing the mass exchange with the environment, including the dissolved and particulate masses in the liquid (influent and effluent) and the mass of gases entering or leaving the reactor, according to meteorology.

The model consists in four coupled dynamical equations, whose structure is illustrated in Figure 2. Each subsystem represents the dynamics of the

biochemical species (Equation (1)), of the reactor volume (Equation (2)), of the temperature (Equation (3)) and of $\hat{H}^+$ ions (Equation (4)):

$$\dot{\xi} = K \cdot \rho(\xi, T, \theta, \hat{H}^+) + \Delta(\xi, \xi_{in}, T, \hat{H}^+) \quad (1)$$

$$\dot{V} = Q_{in} - Q_{out} + Q_{rain} - Q_{evap} \quad (2)$$

$$\dot{T} = \sum_j Q_i(T, \theta, \rho) \quad (3)$$

$$\dot{\hat{H}}^+ = \hat{K}\left(\Phi_{\mathrm{pH}}\left(\hat{H}^+, \xi, T\right) - \hat{H}^+\right) \quad (4)$$

Where ξ represents the set of state variables associated with dissolved (denoted S_{YY} according to the IWA convention) or particulate (denoted X_{YY} according to the IWA convention) compounds, $[g.m^{-3}]$. $K = P^T$ is the stoichiometric matrix (P being the Petersen matrix). $\rho(\xi)$ is the vector of the biological reaction rates $[g.m^{-3}.d^{-1}]$. The vector of fluxes from and towards the environment (considering all the phases: solid, liquid and gaseous) is denoted Δ. ξ_{in} is the vector of influent concentrations $[g.m^{-3}]$.

The reactor volume V depends on Q_{in}, Q_{out}, Q_{rain} and Q_{evap}, respectively the inflow rate, outflow rate, rain rate and evaporation rate $[m^3 d^{-1}]$; Finally, the vector T contains the temperature of the key elements of the process. In the applied example to algae-bacteria systems, the vector T includes the temperature of the water body and the one of the concrete envelope in contact with the ground. The various heat fluxes are denoted Q_h, i. These fluxes depend on the meteorological variables vector $\theta(t)$, including solar heat flux,

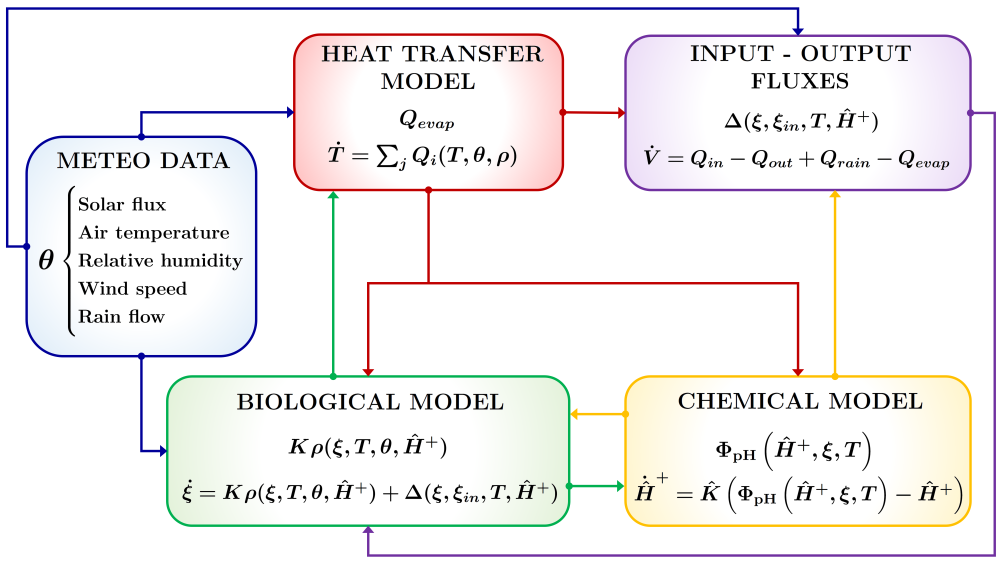

Figure 2: General FLAME modelling framework for full predictions from meteorological data

air temperature, wind speed, rain rate and relative humidity.

The meteorological data are used for simulating the dynamics of the medium temperature, but also for determining the light availability and distribution in the medium and also the evaporation rate.

The last term represents the system to be solved for simulating the pH dynamics through the computation of $\hat{H^+}$ $(mol.m^{-3})$. This term contains an algebraic equation system involving all the ionic species dissociation and mass balances, $\Phi_{\mathrm{pH}}([\hat{H^+}], \xi, T)$. The convergence rate of $\hat{H^+}$ towards H^+, the actual proton concentration, is $\hat{K}$, with a faster time-scale compared to the biological process rates. The chemical submodel, which depends on the reactor temperature, is necessary to compute the molecular speciation, and

thus the biological reaction rates. A more detailed description of the heat transfer model and the chemical sub-model can be found in sections 3.4 and 3.5.

Finally, a module computes the flux of compounds Δ from and towards the environment external to the reactor. It consists in considering the flux of soluble elements in the influent and effluent, the flux of solids (which have been possibly recirculated or harvested) and the flux of gases exchanged with the liquid phase (the speciation of the dissolved compounds, e.g. CO_2 and NH_3, quantified through the chemical model).

4.2. The biological core model

4.2.1. Mass balance structure of biological models

The classical structure of mass balance models for perfectly mixed bioreactors consists in representing the mass transfer taking place between the n_ξ state variables, through a set of n_ρ reactions (Bastin and Dochain, 1990; Dochain and Vanrolleghem, 2001): $K \cdot \rho(\xi, T, I, [H^+])$

The underlying reaction network is represented by the stoichiometric matrix K. Each column of this matrix correspond to a (macroscopic) reaction. It is recommended that this reaction network conserves the elemental masses (at least of C, N and P). The choice of the number of microbial species is delicate and will definitely orientate the modelling, balancing accuracy and complexity.

The two bricks of the biological model (reaction network and reaction

kinetics) must be chosen with care, and this is the most difficult step in developing a biological model (Mairet and Bernard, 2019).

The biological kinetics are affected by medium temperature (T_R), light intensity, nutrient concentrations and pH. Appendix B recalls some standard kinetics to represent these effects. For all the above mentioned reasons, designing the biological model is a time demanding task. It is, however, the core of the bioreactor dynamics and also the key for a further successful use of the model for advanced control.

The main advantage of the proposed FLAME framework is that it is straightforward to replace the biological core model, keeping the same chemical, heat transfer and input/output model. Various competitive biological models can then be implemented, comparing the inherent ability to well represent the process, independently of the heat-transfer or chemical framework which stay unchanged (see Table 1). It is also the opportunity to benefit from different models which all together can contribute to improve predictions by proposing a coherent predictive framework (Mairet and Bernard, 2019).

As a matter of illustration, we present hereafter the fully predictive ALBA model, according to the FLAME framework structure.

4.3. Example of the ALBA biological core model

A first version of the ALBA model has already been proposed to represent algae-bacteria systems for wastewater remediation (Casagli et al., 2021b,a). The ALBA model (Casagli et al., 2021b), simulates the dynamics of an out-

door algae-bacteria raceway. The biological sub-model considers a mixed culture of algae (X_{ALG}), heterotrophic bacteria (X_H), Ammonium Oxidizing Bacteria (X_{AOB}) and Nitrite Oxidizing Bacteria (X_{NOB}). The model includes 19 biological processes and involves 17 state variables. The associated stoichiometric matrix (see Appendix D) has been computed so as to balance elemental C, N, P, O and H.

In Appendix C we recall the main choices made in the construction of the model. We refer the reader to Casagli et al. (2021b,a) for more details.

The model was successfully calibrated and validated using the dataset relative to a demonstrative scale raceway treating synthetic municipal wastewater (see Appendix A) located in Narbonne (France) and a pilot-scale raceway treating piggery digestate located in Milano (Italy).

Altogether, 30 days were exploited for the calibration phase (from Narbonne case study), while 602 days were used validating the model (from Narbonne and Milan case study) based on a set of experimental data (pH, S_{O2}, S_{NH}, S_{NO3}, S_{NO2}, X_{ALG}, TSS and soluble COD).

At this stage, the ALBA model requires a measurement of the reactor temperature to run. The proposed FLAME framework extends this model to make it fully predictive, *i.e.* depending only on the local meteorological data.

4.4. Heat transfer model to predict the reactor temperature

Here we focus on reactors with an active mixing that guaranties that the biochemical concentrations and temperatures are homogeneous in the water body. We can therefore take benefit from the universal temperature model for high rate ponds developed by Béchet et al. (2011) to predict the water temperature and the water level of the reactor. However this model has two hindrances. First, implementing the temperature profile in the ground is complex, making it difficult to use. Second, as it can be seen in Béchet et al. (2018), it underestimates the actual thermal inertia of the system, simulating temperature fluctuations with a too large amplitude. The temperature model of Béchet et al. (2011) was thus modified to account for the inertia of the reactor support (assumed to be concrete in this case), especially at the bottom under the liquid mass. An overall heat balance was then carried out on the support, adding an equation describing its temperature evolution. The considered heat fluxes for the water mass and the support are illustrated on Figure 3.

The first heat balance considers the temperature dynamics in the reactor, accounting for the heat exchanges with the material of the reactor :

$$\begin{aligned} \rho_w V C_{p,w} \frac{dT_R}{dt} &= Q_{ra,p} + Q_{ra,s} + Q_{ra,a} + Q_{h,evap} + Q_{conv} + Q_{h,in} \\ &\quad + Q_{h,out} + Q_{h,rain} - Q_{conv,cond_w,co} \end{aligned} \tag{5}$$

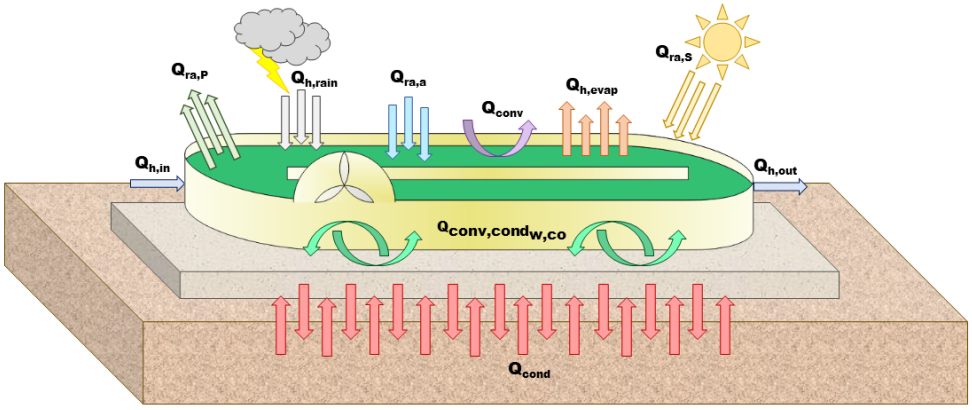

Figure 3: Heat balance on both water and reactor bodies and interaction with the ground.

where: T_R is the medium temperature in the reactor (K); ρ_w is the density of the water (kg m^{-3}); C_{pw} is the specific heat capacity of the water (J kg^{-1} K^{-1}); and V is the water volume (m^3). $Q_{ra,p}$ is the radiation from the reactor surface (W); $Q_{ra,s}$ is the total (direct + diffuse) solar radiation (W); and $Q_{ra,a}$ is the radiation from the air to the water (W). $Q_{h,evap}$ is the evaporation flux (W), Q_{conv} is the convective flux at the water surface (W); $Q_{h,in}$ (resp. $Q_{h,out}$) is the heat flux associated with the influent (resp. effluent) water (W); and $Q_{h,rain}$ is the heat flux related to rain [W].

The term $Q_{conv,cond_w,i}$ is the conductive/convective flow related to the heat exchange between water and concrete:

$$Q_{conv,cond_w,co} = h_{w,co} \cdot (T_R - T_{co}) \tag{6}$$

The parameter $h_{w,co}$ (W m^{-2} K^{-1}) is the heat transfer coefficient between the water (w) and the reactor support (co), and T_{co} (K) is the temperature of the concrete.

The differential equation describing the temperature dynamics of the concrete of the support is:

$$\rho_{co} V_{co} C_{p,co} \frac{dT_{co}}{dt} = h_{w,co} \cdot (T_R - T_{co}) + Q_{cond} \tag{7}$$

where Q_{cond} is the conductive heat flux with the ground at the reactor bottom (W). The conductive flux has a minor impact on the total heat balance (Béchet et al., 2011), therefore, a linear soil temperature profile was implemented for sake of simplicity, assuming that the ground temperature was approximately equal to the annual average air temperature at a depth of 3.5 meters.

The evaporative and convective heat flux have a strong effect on the temperature prediction, and they were implemented according to the Buckinngham theorem, depending on the dimensionless numbers of Sherwood, Schmidt and Reynolds. The Sherwood and Nusselt numbers were linearly interpolated for Reynolds numbers between 3×10^5 and 5×10^5 to ensure model calculations for Reynolds numbers in the transition from laminar to turbulent flow. To avoid a zero evaporation when there is no wind, a minimum wind speed (4

m s^{-1}) was considered in the calculation of the evaporative heat flux.

For the processes where the biological activity is associated to exothermic reactions, a heat flux must be added proportional to the biological kinetics. This is especially important for the exothermic heterotrophic bacteria growth in activated sludge (Sedory and Stenstrom, 1995).

Also, a more suitable model for the conduction between the concrete envelope and the ground must be implemented, when the tank is partially buried, as for aeration basins (Sedory and Stenstrom, 1995).

4.5. General principle of the chemical sub-model

In most of the bioprocesses there is a broad range of involved molecules, including species whose speciation depends on pH. It is therefore crucial to well represent the pH and the dissociation state of the key chemical species which affect the biological kinetics and the exchange with the environment.

For most of the models, this analysis is often carried out considering a limited number of chemical species and using directly the measured pH to estimate the chemical speciation in the reactor. The framework that we propose is general and can be straightforwardly adapted to most of the case studies.

The sub-model for pH prediction (H^+ ions concentration) results from the dynamical balance between the chemical, physical and biological process interactions. The proposed pH sub-model is based on dissociation equilibria and mass balances of acids and bases, extending the one proposed in the

ADM1 model and on the charge balance, through which the concentration of hydrogen ions is computed. Here the main contribution is the method to systematically write the problem and to solve the algebraic equations system. In the proposed pH model polyprotic acids speciation are considered, given the wide range of pH variation (when it is not controlled) due to the photosynthetic activity, while in ADM1 only monoprotic acids were integrated.

The chemical submodule includes three components, represented in Table 2 which must be tailored to the specific case:

1. The mass balance equations for the state variables of the biological model, which correspond to the sum of chemicals which dissociate in the water. As an example to describe the total concentration of CO_2, HCO_3^- and CO_3^{2-} in the ALBA model correspond to the state variable inorganic carbon (denoted S_{IC} in the ALBA model):

$$\frac{S_{IC}}{12} = CO_2 + HCO_3^- + CO_3^{2-}$$

   Note that this equation can also account for the change in unit between the state variables ($g.m^{-3}$) and the chemical model (which should be in $mol.m^{-3}$).

2. The dissociation equations based on the affinity constants. They must be rewritten in a form where only the H^+ ions concentration together with the total amount of the element appears (represented by one of the model state variable). For example, for the dissociation constant

associated with the CO_2 equilibrium:

$$H_2O + CO_2 \rightleftharpoons HCO_3^- + H^+$$

we get:

$$CO_2 = \frac{S_{IC}/12}{1 + \frac{Ka_{CO_2}10^3}{H^+} + \frac{Ka_{CO_2}Ka_{HCO_3}10^6}{(H^+)^2}} \tag{8}$$

with $K_{A,H_2CO_3} = 4.27E{-}07M$.

And for the dissociation constant associated with the HCO_3^- equilibrium:

$$HCO_3^- \rightleftharpoons CO_3^{2-} + H^+$$

$$HCO_3^- = \frac{S_{IC}/12}{1 + \frac{H^+}{Ka_{CO_2}10^3} + \frac{Ka_{HCO_3}10^3}{H^+}} \tag{9}$$

with $K_{A,HCO_3} = 4.68E{-}11$.

3. The ionic balance equation representing the electroneutrality of the medium, accounting for all the ions that are affected by the reactions, and for those of constant concentration (denoted $\Delta_{CAT,AN}$) whose concentrations are not modified by any biochemical reaction. As a matter of illustration for WWT processes, a general electroneutrality

equation is:

$$\begin{aligned} H^+ + NH_4^+ + \Delta_{CAT,AN} = \; & OH^- + NO_2^- + NO_3^- + HCO_3^- \\ & +2CO_3^{2-} + H_2PO_4^- + 2HPO_4^{2-} \\ & +3PO_4^{3-} + C_2H_3O_2^- + C_3H_5O_2^- + C_4H_7O_2^- \end{aligned}$$

Note that the notion of Total Alkalinity (TA) (mol m^{-3}) is directly derived from these considerations, as reported by Casagli et al. (2021a):

$$\begin{aligned} TA \; = \; & HCO_3{}^- + 2CO_3^{2-} + H_2PO_4^{2-} \\ & +2PO_4^{3-} + OH^- + NH_3 + C_2H_3OO^- \\ & +C_4H_7OO^- + C_3H_5OO^- + C_5H_9OO^- + HS^- \\ & +2S^{2-} - H^+ - HNO_2 - HNO_3 - H_3PO_4 \end{aligned} \tag{10}$$

Temperature has a fundamental influence on the parameters of chemical equilibria (i.e. the acidity constants), as specified by Batstone et al. (2002). This effect must be implemented for adapting the model for speciation to temperature oscillations (especially for the processes running along all the year). See Appendix G for the detailed expressions of the temperature dependencies.

4.5.1. Chemical sub-model for the ALBA model

As a matter of illustration, the chemical sub-model for the ALBA model follows the presented structure, considering the equilibria and mass conservation presented in Table 2. The ALBA model was validated also on a six months dataset of a raceway treating digestate. Since the digestate can

present significant concentrations of volatile fatty acids (VFA - acetate, butyrate, propionate and valerate) and hydrogen sulphide (H_2S), in that case the algebraic equation system for the chemical equilibria should take them into account, as proposed in Table J.4 (see Appendix J). As explained by Batstone et al. (2002), the Van't Hoff equation is not effective for organic acids. However, their acidity constants only marginally vary in the temperature range 0-60 °C.

Table 2: (Part I) Algebraic equations for the chemical sub-model: mass balances and dissociation state

Description	Expression $[molm^{-3}]$	K_A [M]
	Ammoniacal nitrogen	
1) Mass balance	$\frac{S_{NH}}{14} - NH_3 - NH_4^+ = 0$	
2) Dissociation		
$NH_4^+ \rightleftharpoons NH_3 + H^+$	$NH_4^+ - \frac{S_{NH}/14}{1+\frac{Ka_{NH_4}10^3}{H^+}} = 0$	$K_{A,NH_4^+} = 5.62E{-}10$
	Nitrogen oxides	
3) Mass balance	$\frac{S_{NO_2}}{14} - NO_2^- - HNO_2 = 0$	
4) Dissociation		
$HNO_2 \rightleftharpoons NO_2^- + H^+$	$HNO_2 - \frac{S_{NO_2}/14}{1+\frac{Ka_{HNO_2}10^3}{H^+}} = 0$	$K_{A,HNO_2} = 4.47E{-}04$
5) Mass balance	$\frac{S_{NO_3}}{14} - NO_3^- - HNO_3 = 0$	
6) Dissociation		
$HNO_3 \rightleftharpoons NO_3^- + H^+$	$HNO_3 - \frac{S_{NO_3}/14}{1+\frac{Ka_{HNO_3}10^3}{H^+}} = 0$	$K_{A,HNO_3} = 4.37E{+}01$
	Inorganic carbon	
7) Mass balance	$\frac{S_{IC}}{12} - CO_2 - HCO_3^- - CO_3^{2-} = 0$	
8) Dissociation		
$H_2O + CO_2 \rightleftharpoons HCO_3^- + H^+$	$CO_2 - \frac{S_{IC}/12}{1+\frac{Ka_{CO_2}10^3}{H^+}+\frac{Ka_{CO_2}Ka_{HCO_3}10^6}{(H^+)^2}} = 0$	$K_{A,H_2CO_3} = 4.27E{-}07$
9) Dissociation		
$HCO_3^- \rightleftharpoons CO_3^{2-} + H^+$	$HCO_3^- - \frac{S_{IC}/12}{1+\frac{H^+}{Ka_{CO_2}10^3}+\frac{Ka_{HCO_3}10^3}{H^+}} = 0$	$K_{A,HCO_3} = 4.68E{-}11$

Table 1: (Part II) Algebraic equations of the chemical sub-model: mass balances and dissociation state

	Ortophosphates	
10) Mass balance	$\frac{S_{PO_4}}{31} - H_3PO_4 - H_2PO_4^- - HPO_4^{2-} - PO_4^{3-} = 0$	
11) Dissociation $H_3PO_4 \rightleftharpoons H_2PO_4^- + H^+$	$H_3PO_4 - \frac{S_{PO_4}/31}{1+\frac{Ka_{H_3PO_4}10^3}{H^+}+\frac{Ka_{H_3PO_4}Ka_{H_2PO_4}10^6}{(H^+)^2}+\frac{Ka_{H_3PO_4}Ka_{H_2PO_4}Ka_{HPO_4}10^9}{(H^+)^3}} = 0$	$K_{A,H_3PO_4} = 7.24E{-}03$
12) Dissociation $H_2PO_4^- \rightleftharpoons HPO_4^{2-} + H^+$	$H_2PO_4^- - \frac{S_{PO_4}/31}{1+\frac{H^+}{Ka_{H_3PO_4}10^3}+\frac{Ka_{H_2PO_4}10^3}{H^+}+\frac{Ka_{H_2PO_4}Ka_{HPO_4}10^6}{(H^+)^2}} = 0$	$K_{A,H_2PO_4} = 6.17E{-}08$
13) Dissociation $HPO_4^{2-} \rightleftharpoons PO_4^{3-} + H^+$	$HPO_4^{2-} - \frac{S_{PO_4}/31}{1+\frac{(H^+)^2}{Ka_{H_3PO_4}Ka_{H_2PO_4}10^6}+\frac{H^+}{Ka_{H_2PO_4}10^3}+\frac{Ka_{HPO_4}10^3}{H^+}} = 0$	$K_{A,HPO_4} = 2.14E{-}13$
14) Dissociation $H_2O \rightleftharpoons OH^- + H^+$	$OH^- - \frac{Ka_w 10^3}{H^+}$	$K_{A,HPO_4} = 1.00E{-}14$
15) Charge balance	$H^+ + NH_4^+ + \Delta_{CAT,AN} - OH^- - NO_2^- - NO_3^- - HCO_3^- - 2CO_3^{2-} - H_2PO_4^- - 2HPO_4^{2-} - 3PO_4^{3-} = 0$	

4.5.2. Chemical sub-model resolution

The strategy for resolving the pH subsystem was inspired by Rosén and Jeppsson (2006), extending it to polyprotic acids. The idea was to transform the problem of resolution of a set of algebraic equations given in Table 1 into the solution of a differential system. The way this system is solved, with the example of the ALBA model is proposed in Appendix K.

4.6. I/O fluxes from and towards the environment

This module manages the exchanges of liquid, solid and gaseous fluxes from and towards the environment. The liquid and solid fluxes are associated to hydraulic retention time (HRT) and solid retention time (SRT) respectively. HRT and SRT can differ in reactors where biomass is fixed to a support, or with a separation system such as membranes. A submodel of the different fluxes (recirculation, harvesting,...) is then needed.

The outflow of gases for which the dissolved molecules are at higher concentration than the solubility constant, or the inflow of gases at a lower concentration than the solubility constants must be taken into account

The CO_2, O_2 stripping/dissolution, but also of other gases such as volatile fatty acids or NH_3 must be considered, quantifying their rates through the k_La and their diffusion coefficients (D_{S_j}):

$$Q_j = k_L a_j(T_R) \cdot \left(\frac{D_{S_j}}{D_{S_{O_2}}} \right)^2 \cdot (S_{j,sat}(T_R) - S_j) \tag{11}$$

Finally, the flux of water by evaporation must also be quantified, as com-

puted by the heat transfer model, see Equation (12).

It becomes then possible to evaluate the water level variation, and then the reactor volume:

$$S\frac{dh_L}{dt} = -\frac{m_e}{\rho_w} + Q_{rain} + Q_{in} - Q_{out} \tag{12}$$

where m_e is the evaporation rate ($Kg.s^{-1}m^{-2}$); ρ_w is the water density ($Kg.m^{-3}$); Q_{rain} is the rain rate (ms^{-1}); Q_{in} and Q_{out} are the inflow and outflow rate, respectively. ($m^3.s^{-1}$).

5. Results and discussion

5.1. Fully predictive ALBA model validation on an outdoor demonstrative-scale

Simulations were run using all the model compartments within the FLAME framework, in order to compare the fully predictive model accuracy with the simulations based on the measured pond temperature.

First, the physical sub-model dealing with temperature turns out to accurately predict the temperature dynamics on a long time scale (443 days). The temperature predictions properly follow the seasonal variation trend (figure 4 and Table 2). The predicted temperature oscillations slightly overestimate or underestimate the measurements along the validation period, with an average error standard deviation of 1.44° C. Considering all the experimental period, the heat transfer model remains very accurate, with a R^2 of 0.96,

computed on 10555 measurement points, and p-value lower than 1E-06. The heat transfer model was simulated using the nearby meteorological data 30 km away. Given the great influence of some input data on simulation results (e.g: total irradiance, air temperature and wind velocity) model predictions could be further improved by collecting data from a meteorological station located exactly at the pond location, therefore providing a more accurate description of the onsite environmental conditions.

The biological response for the most relevant variables of the algae-bacteria pond for the fully predictive ALBA model are reported in figure 7 and Table 2. The experimental measurements of S_{NH}, S_{NO2}, S_{NO3}, S_{O2}, pH, TSS, X_{ALG} and COD_S are shown together with their standard deviation, while the fully predictive model simulations are shown together with their error bounds, computed according to the procedure presented by Casagli et al. (2021b). In addition, in table 2, different model goodness of fit are reported, in order to more accurately depict the difference between the full predictive framework and the simulations based on temperature measurements.

The fully predictive ALBA model was able to simulate the main measured variables in the HRABP with a very good level of accuracy, being very close to the ones obtained when running the model with the measured temperature. As reported in Table 2, all the computed criteria confirmed the model goodness of fit.

An advantage of an accurate mathematical model is its ability to reconstruct the components of the microbial population, and the relative distri-

a)

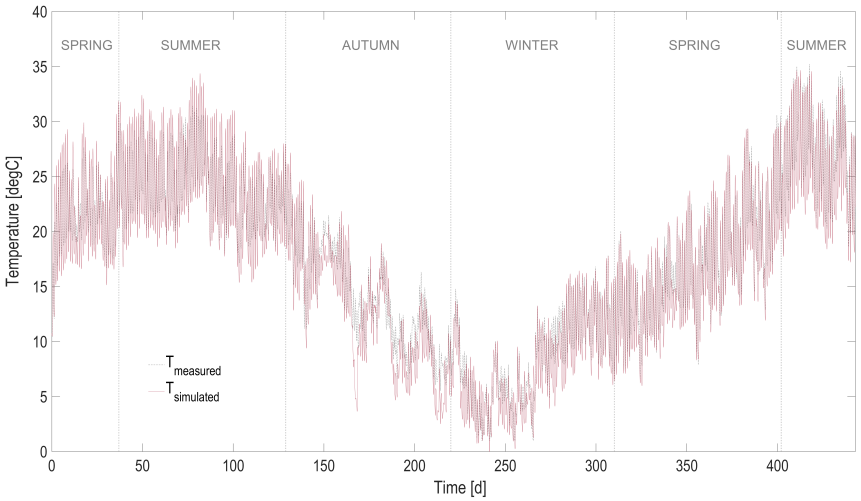

b)

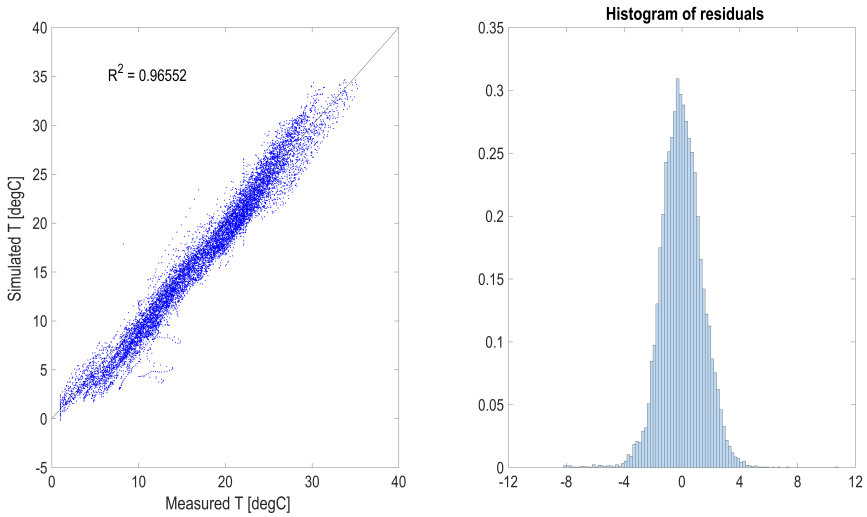

Figure 4: Heat transfer model validation over one year experimental measurements

bution between microalgae, heterotrophic bacteria and nitrifiers (AOB and NOB). Direct measurements with phylogenetic markers (Junier et al., 2010) would be challenging over a full year. Figure 5 shows how the microbial population partitioning is shaped by the seasons. Microalgae dominate the population along the year. During Spring and Summer the algal biomass, being stimulated by higher temperatures and light intensities, it reaches the highest average concentrations (348-367 $gCODm^{-3}$), while it is twofold reduced in Autumn and Winter (200-171 $gCODm^{-3}$). The biomass of heterotrophs stays at a constant level along all the seasons (60-93 $gCODm^{-3}$). Nitrifiers are 50 times less abundant compared to the other biomasses, and they exhibit a very different trend. AOB and NOB reach the highest concentration levels in Summer and Autumn (4.9-5.1 $gCODm^{-3}$ for AOB and 1-1.2 $gCODm^{-3}$ for NOB). The nitrifying biomass is reduced twofold in Winter, where temperatures are too low for supporting its activity (2.6 $gCODm^{-3}$ for AOB and 0.4 $gCODm^{-3}$ for NOB). The biomass composition is different when the ecosystem is fed with digestate (see the case study presented in Appendix F, figure F.9). AOB and NOB concentrations are higher (16-33 $gCODm^{-3}$ for AOB and 5-7 $gCODm^{-3}$ for NOB in summer and autumn, respectively), due to the increased influent ammoniacal nitrogen concentration, exacerbated by the longer biomass retention time. Nitrifiers are responsible for the main nitrogen fluxes. The heterotrophic bacteria concentration is much lower (17-22 $gCODm^{-3}$ in summer and autumn, respectively) compared to the previous case, probably due to the reduced influent biodegradable organic matter

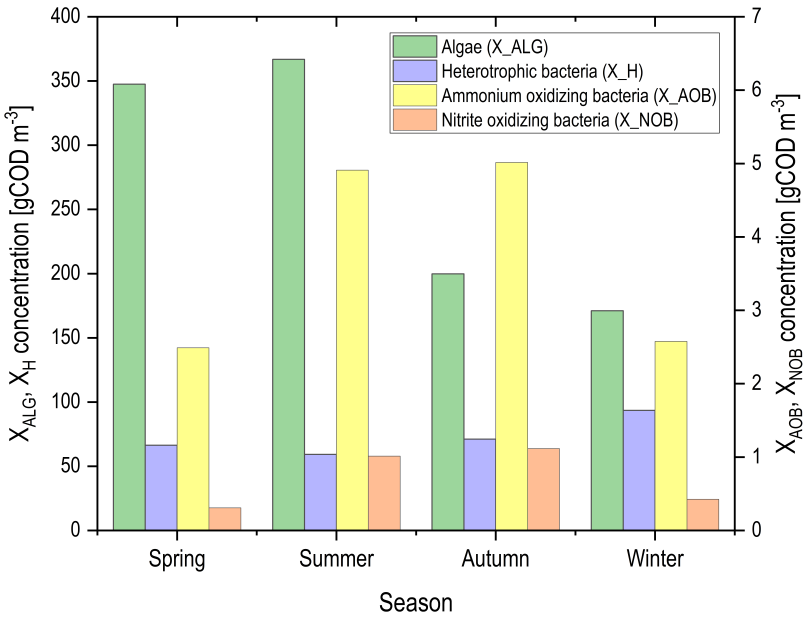

Figure 5: Average composition of the microbial population according to seasons, as estimated by the fully predictive model. Right axis: algae (X_{ALG}) and heterotrophic bacteria (X_H) concentration; left axis: nitrifying bacteria (X_{AOB} and X_{NOB}) concentration.

content. The highest algae concentration is reached again during Spring and Summer (498-592 $gCODm^{-3}$, respectively). These values are higher compared to the previous case. This is probably due to pH regulation with CO_2 injection, avoiding inorganic carbon limitation during the light periods.

5.2. How temperature affects alkalinity in HRABP

From the results shown in figure 7 and Table 2, it can be noticed that nitrate and nitrite predictions turn out to be sensitive to small biases in temperature simulations. This is possibly due to: i) the very low concentration of nitrifiers in this system, compared to the algal and heterotrophic

bacterial biomass, and ii) the high sensitivity of AOB and NOB to temperature oscillations, being typically slow growers and therefore requiring more time for adapting to oscillating environmental conditions. The difference between nitrate simulated with both models resulted in a reduced R^2 and a higher average relative error. The experimental data and the simulations run based on temperature measurements, show a nitrate drop after reaching a pick at day 410. For nitrate predicted in the FRAME framework, this descendent trend is less marked and nitrate remain around an average concentration of 26 gNm^{-3}. This is due to the higher predicted X_{NOB} concentration (1.12 $gCODm^{-3}$ in average) compared to the one simulated using the measured temperature (0.85 $gCODm^{-3}$ in average). The explanation of this phenomenon can be found in the temperature dependence function of X_{NOB} growth rate, which peaks at $T_{opt} = 20^{\circ}$ C. Since the predicted temperature, especially during night, slightly underestimates the real one, a temperature closer to the optimal T_{opt} is simulated, enhancing the X_{NOB} growth kinetic. This effect is amplified by the low concentration of nitrifiers, while it is not producing significant variation for the other biomasses, whose concentrations are one or two orders of magnitude higher.

It is worth remarking that the sensitivity of nitrifiers to temperature have already been noticed (la Cour Jansen et al., 1992) and the challenges to operate reactors at low temperature motivated the pioneer development of heat transfer models to predict temperature dynamics.

The computed model error bars appropriately indicate this sensibility

during this period. The experimental data stay therefore within the model uncertainty range (figure 7c). In the same period where X_{NOB} activity is overestimated, the simulated total alkalinity (see Equation 10), resulted to be slightly lower compared to the one simulated using the measured temperature. The central role played by total alkalinity was shown by Casagli et al. (2021a), and especially how it affects the level of inorganic carbon in the system. Alkalinity must stay sufficiently high to allow a pool of inorganic carbon that can support algae and nitrifiers activity. It is of utmost importance to avoid competition for inorganic carbon between these two populations, leading to favourable conditions for N_2O production and emissions. Therefore, large errors in predicting the pond temperature can bring to erroneous estimations of the distribution between ammonium, nitrate and nitrite. It follows that alkalinity estimation will be biased and consequently inorganic carbon concentration in the pond, with an overall uncertainty on the N_2O emissions. The nitrifying activity was moderate (Casagli et al., 2021b) for this case study, where the influent ammoniacal nitrogen is at low concentration ($S_{NH_{in}}$=8 gNm^{-3}), compared to the organic nitrogen fraction ($S_{ND_{in}}$=60 gNm^{-3}). Therefore no mechanisms of competitions for inorganic carbon between algae and nitrifiers were observed. However, when studying HRABPs treating digestate, as the one reported in Casagli et al. (2021a), a very strong limitation for inorganic carbon caused by a drop in alkalinity due to a strong nitrifying activity can be observed, despite the presence of a pH control with CO_2 bubbling. In these cases, an approximate and raw

estimation of the pond temperature, might lead to a large bias in alkalinity predictions, resulting in inefficient optimization strategies, potentially associated with a risk of N_2O emission.

State variable	Err.St.Dev. (av)	TIC. (-)	Coeff.Var. (-)	R^2 (-)
S_{NH}	0.5435	0.0905	0.2254	0.98988
S_{NO2}	2.4545	0.1573	0.4659	0.95893
S_{NO3}	4.948	0.1962	0.323	0.86162
X_{ALG}	6.824	0.0224	0.0242	0.99582
TSS	8.6835	0.029	0.03	0.98365
$CODs$	2.5589	0.0435	0.0465	0.95819
S_{O2}	0.7025	0.1163	0.0778	0.95861
pH	0.2663	0.0336	0.0292	0.93236
T^*	1.4477	0.081	0.0833	0.96552

Table 2: Comparison between simulation results using temperature measurement and temperature predictions from the heat transfer model. The error standard deviation, the absolute relative error, the variation and the correlation coefficients are computed. (*): for temperature, the comparison is between the experimental measurements and the predicted pond temperature with the heat transfer model.

5.3. Opening the door for Model Predictive Control

Model Predictive Control (MPC) is an advanced control approach (Camacho and Alba, 2013; Hewing et al., 2020) for enhancing the process efficiency by running a wide range of scenarios and selecting, among the ones satisfying some constraints, the ones offering the best performances. Combined with weather forecasts, this approach can even anticipate the effect of the meteorological evolution (De-Luca et al., 2017, 2019).

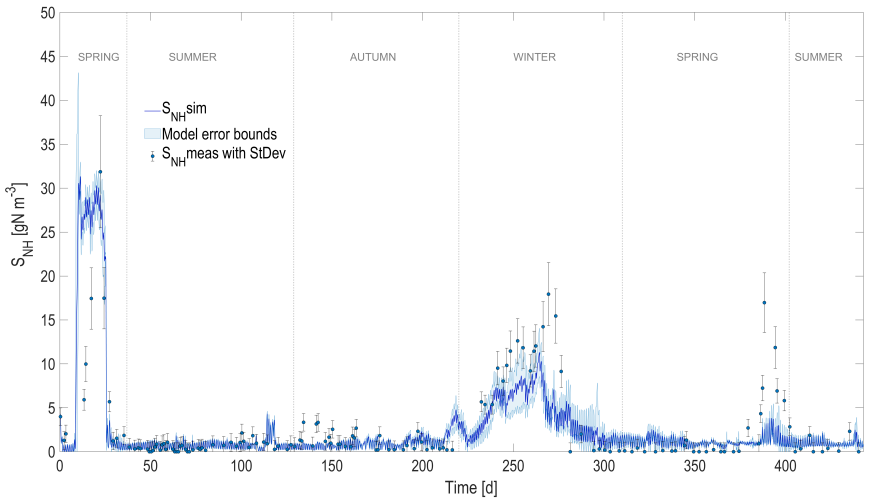
SPRING
SUMMER
AUTUMN
WINTER
SPRING
SUMMER
S_NH sim
Model error bounds
S_NH meas with StDev
S_NH [gN m-3]
Time [d]

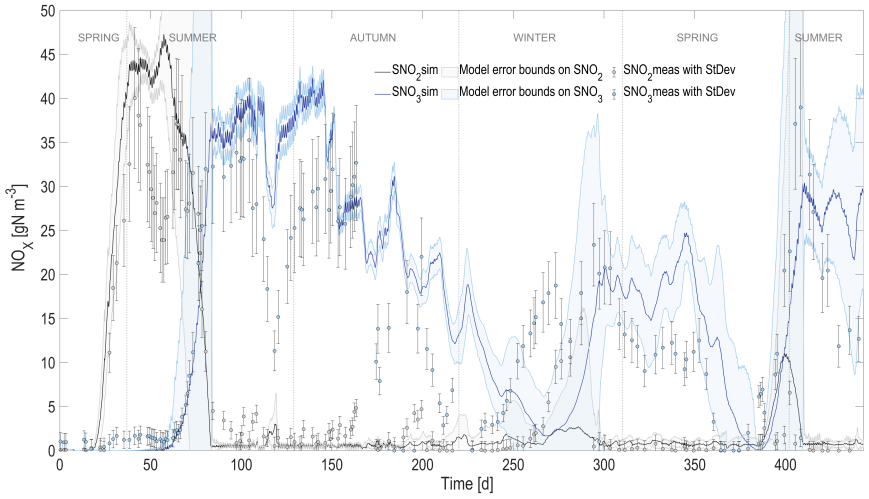
SPRING
SUMMER
AUTUMN
WINTER
SPRING
SUMMER
SNO2 sim
SNO3 sim
Model error bounds on SNO2
Model error bounds on SNO3
SNO2 meas with StDev
SNO3 meas with StDev
NOX [gN m-3]
Time [d]

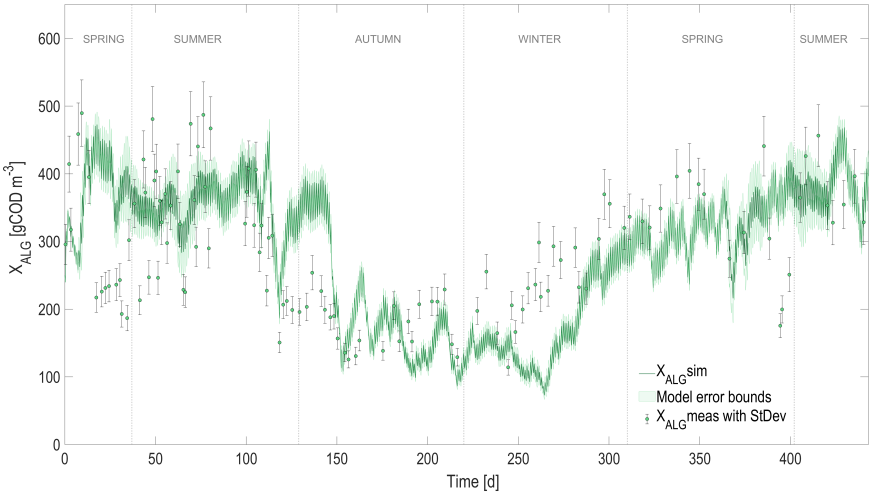
SPRING
SUMMER
AUTUMN
WINTER
SPRING
SUMMER
X_ALG sim
Model error bounds
X_ALG meas with StDev
X_ALG [gCOD m-3]
Time [d]

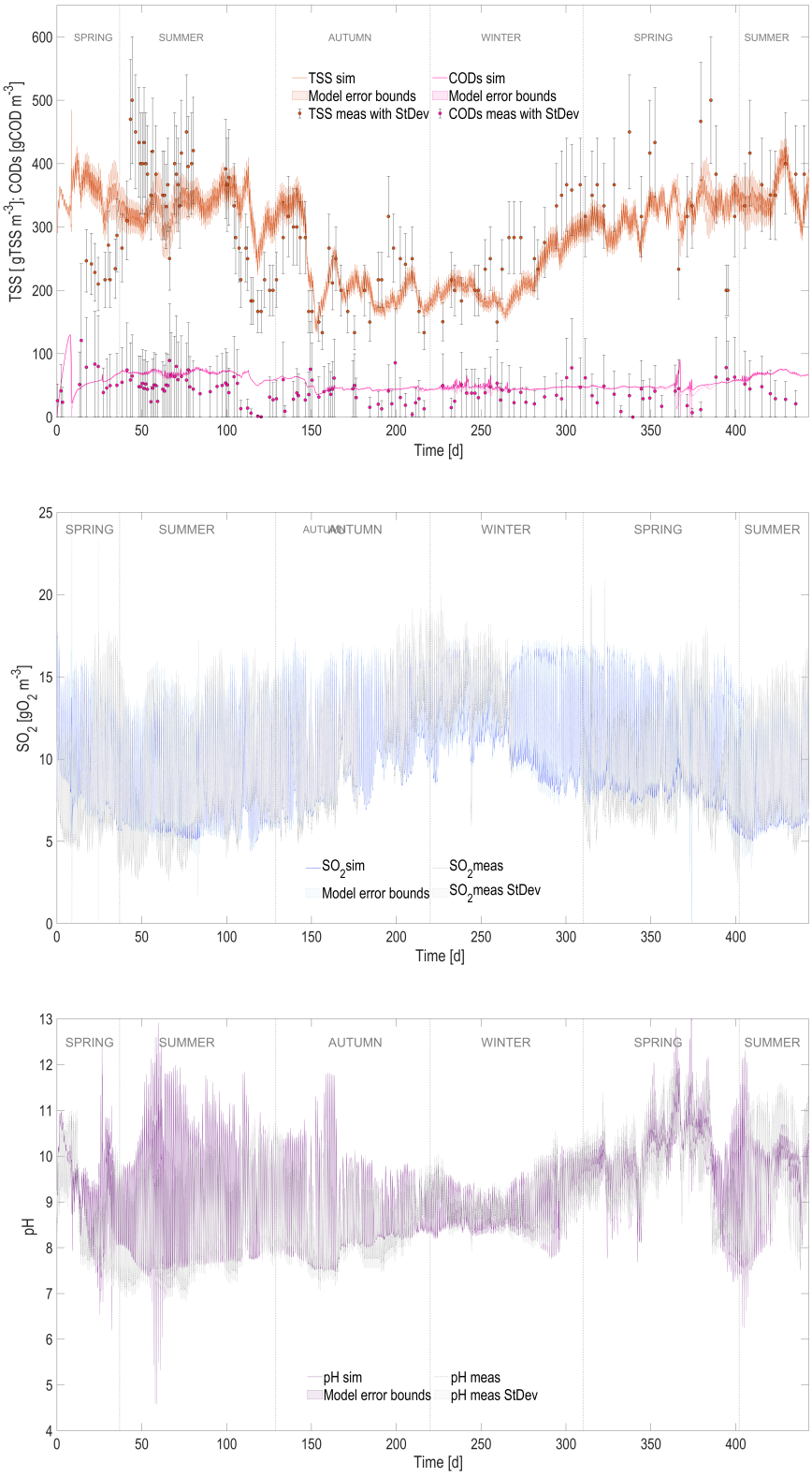

Figure 7: ALBA fully predictive model validation over one year. Experimental measurements and their Standard deviation, Error bounds for model predictions and simulation results: a) ammoniacal nitrogen; b) nitrite and nitrate; c) algal biomass; d) total suspended solids and soluble COD; e) dissolved oxygen; f) pH.

De-Luca et al. (2017, 2019) implemented a MPC strategy based on a simple model accounting for temperature evolution in a mono-specific culture of microalgae. By efficiently managing temperature and light use, it resulted in doubling algal productivity. This was achieved by on-line controlling the water depth to anticipate the weather fluctuations and to better manage the hottest periods in summer. The FLAME framework makes it possible to apply similar strategies for more complex environmental processes.

The model can specifically be used to assess the sensitivity of outdoor biotechnological processes to temperature. It is capital to better understand which are the variables most affected by temperature. This also means that the temperature predictions must be accurate for an efficient decision-making process and for optimization. A biased temperature prediction at industrial scale can be critic for these variables resulting in a degradation in the control performance or leading to inappropriate decisions.

As a matter of illustration, for the algae/bacteria process, nitrifiers turned out to be highly temperature sensitive. Accurately representing this population is difficult, yet crucial to get a good description of ammonium, nitrate and nitrite concentrations. A biased prediction of these quantities induces a wrong alkalinity estimation, with potential risk of inorganic carbon limitation and then the risk of N_2O emission. For these variables, it is thus key that the model is sufficiently accurate to make the management strategy efficient in terms of wastewater remediation efficiency, nutrients recovery, and also of greenhouse gas emissions.

6. Conclusions

Temperature is a key factor affecting the enzymatic processes and shaping the microbial communities. Medium temperature dynamics must be therefore accurately forecast, and also the way it affects the various biological process represented.

The FLAME framework reveals to be particularly efficient to predict the overall dynamics of an algae-bacteria process over 443 days. The proposed heat transfer model, including the kinetic of both the liquid medium and the reactor envelope is promising for better representing perfectly mixed reactors in a WWTP.

The different models presented in Table 1 all could benefit from the FLAME framework to become fully predictive. Coupled with weather forecasts, they can support a new generation of optimization strategies.

The FLAME framework also offers an opportunity to compare competitive biological models that all have been developed to represent the same process. Keeping the same chemical and physical modules, it proposes a normalized way for benchmarking models. Several models can pass the validation test and can then be kept to generate competitive predictions altogether, improving the prediction accuracy, especially in situations far from the calibration set.

The FLAME framework is a tool beyond the research world and can be applied to large scale plants. It can be helpful during the scale-up phase for preliminary economic assessments and for generating the data to support a

life cycle assessment in order to estimate the environmental footprint. It can be used to guide the design and later, the management of outdoor industrial bioprocesses.

Acknowledgments

This work benefited from the support of the ADEME Biomsa project and from the ANR CtrlAB project (ANR-20-CE45-0014).

References

A.Pizzera, Scaglione, D., Bellucci, M., Marazzi, F., Mezzanotte, V., Parati, K., Ficara, E., 2019. Digestate treatment with algae-bacteria consortia: A field pilot-scale experimentation in a sub-optimal climate area. Bioresource Technology 274, 232–243.

Arashiro, L.T., Rada-Ariza, A.M., Wang, M., Van Der Steen, P., Ergas, S.J., 2017. Modelling shortcut nitrogen removal from wastewater using an algal–bacterial consortium. Water Science and Technology 75, 782–792.

Arnell, M., Ahlström, M., Wärff, C., Saagi, R., Jeppsson, U., 2021. Plant-wide modelling and analysis of wwtp temperature dynamics for sustainable heat recovery from wastewater. Water Science and Technology 84, 1023–1036.

Barrera, E.L., Spanjers, H., Solon, K., Amerlinck, Y., Nopens, I., Dewulf, J., 2015. Modeling the anaerobic digestion of cane-molasses vinasse: Exten-

sion of the anaerobic digestion model no. 1 (adm1) with sulfate reduction for a very high strength and sulfate rich wastewater. Water research 71, 42–54.

Bastin, G., Dochain, D., 1990. On-line estimation and adaptive control of bioreactors. Elsevier, New York.

Batstone, D., Keller, J., Angelidaki, R., Kalyuzhnyi, S., Pavlostathis, S., Rozzi, A., Sandersand, W., Siegrist, H., Vavilin, V., 2002. The iwa anaerobic digestion model no.1 (adm1). Water Science Technology 45(10), 65–73.

Béchet, Q., Shilton, A., Guieysse, B., 2013. Modeling the effects of light and temperature on algae growth: state of the art and critical assessment for productivity prediction during outdoor cultivation. Biotechnology advances 31, 1648–1663.

Béchet, Q., Shilton, A., Park, J.B.K., Craggs, R.J., Guieysse, B., 2011. Universal temperature model for shallow algal ponds provides improved accuracy. Environmental Science & Technology 45, 3702–3709.

Béchet, Q., Sialve, B., Steyer, J.P., Shilton, A., Guieysse, B., 2018. Comparative assessment of evaporation models in algal ponds. Algal Research 35, 283–291.

Bernard, O., Remond, B., 2012. Validation of a simple model accounting for light and temperature effect on microalgal growth. Bioresource Technololgy 123, 520–7.

Bertolazzi, E., 2005. A combination formula of michaelis-menten-monod type. Computers & Mathematics with Applications 50, 201–215.

Bougaran, G., Bernard, O., Sciandra, A., 2010. Modeling continuous cultures of microalgae colimited by nitrogen and phosphorus. Journal of theoretical biology 265, 443–454.

Broekhuizen, N., Park, J.B., McBride, G.B., Craggs, R.J., 2012. Modification, calibration and verification of the iwa river water quality model to simulate a pilot-scale high rate algal pond. Water research 46, 2911–2926.

Buaisha, M., Balku, S., Özalp-Yaman, S., 2020. Heavy metal removal investigation in conventional activated sludge systems. Civil Engineering Journal 6, 470–477.

Camacho, E.F., Alba, C.B., 2013. Model predictive control. Springer science & business media.

Casagli, F., Rossi, S., Steyer, J.P., Bernard, O., Ficara, E., 2021a. Balancing microalgae and nitrifiers for wastewater treatment: can inorganic carbon limitation cause an environmental threat? Environmental science & technology 55, 3940–3955.

Casagli, F., Zuccaro, G., Bernard, O., Steyer, J.P., Ficara, E., 2021b. Alba: A comprehensive growth model to optimize algae-bacteria wastewater treatment in raceway ponds. Water Research 190, 116734.

la Cour Jansen, J., Kristensen, G., Laursen, K., 1992. Activated sludge nitrification in temperate climate. Water Science and Technology 25, 177–184.

De Baar, H., 1994. von liebig's law of the minimum and plankton ecology (1899–1991). Progress in oceanography 33, 347–386.

De-Luca, R., Bezzo, F., Béchet, Q., Bernard, O., 2017. Exploiting meteorological forecasts for the optimal operation of algal ponds. Journal of Process Control 55, 55–65.

De-Luca, R., Bezzo, F., Béchet, Q., Bernard, O., 2019. Meteorological data-based optimal control strategy for microalgae cultivation in open pond systems. Complexity 2019.

Dochain, D., Vanrolleghem, P.A., 2001. Dynamical modelling & estimation in wastewater treatment processes. IWA publishing.

Henze, M., Gujer, W., Mino, T., van Loosdrecht, M.C., 2000a. Activated sludge models ASM1, ASM2, ASM2d and ASM3. IWA publishing.

Henze, M., Gujer, W., Mino, T., Van Loosdrecht, M., 2000b. Activated sludge models ASM1, ASM2, ASM2d and ASM3. IWA publishing.

Hewing, L., Wabersich, K.P., Menner, M., Zeilinger, M.N., 2020. Learning-based model predictive control: Toward safe learning in control. Annual Review of Control, Robotics, and Autonomous Systems 3, 269–296.

Janus, T., Ulanicki, B., 2010. Modelling smp and eps formation and degradation kinetics with an extended asm3 model. Desalination 261, 117–125.

Junier, P., Molina, V., Dorador, C., Hadas, O., Kim, O.S., Junier, T., Witzel, K.P., Imhoff, J.F., 2010. Phylogenetic and functional marker genes to study ammonia-oxidizing microorganisms (aom) in the environment. Applied Microbiology and Biotechnology 85, 425–440.

Klemeš, J.J., Varbanov, P.S., Huisingh, D., 2012. Recent cleaner production advances in process monitoring and optimisation. Journal of Cleaner Production 34, 1–8.

Lippi, S., Rosso, D., Lubello, C., Canziani, R., Stenstrom, M., 2009. Temperature modelling and prediction for activated sludge systems. Water Science and Technology 59, 125–131.

Luo, Y., Yao, J., Wang, X., Zheng, M., Guo, D., Chen, Y., 2020. Efficient municipal wastewater treatment by oxidation ditch process at low temperature: Bacterial community structure in activated sludge. Science of The Total Environment 703, 135031.

Mairet, F., Bernard, O., 2019. Twelve quick tips for designing sound dynamical models for bioprocesses. PLoS Computational Biology 15, e1007222.

Makinia, J., Wells, S.A., Zima, P., 2005. Temperature modeling in activated sludge systems: A case study. Water environment research 77, 525–532.

Martínez, C., Mairet, F., Bernard, O., 2018. Theory of turbid microalgae cultures. Journal of theoretical biology 456, 190–200.

Milledge, J.J., 2011. Commercial application of microalgae other than as biofuels: a brief review. Reviews in Environmental Science and Bio/Technology 10, 31–41.

Morel, A., 1988. Optical modeling of the upper ocean in relation to its biogenous matter content (case I waters). J. Geophys. Res. Ocean. 93, 10749–10768. URL: https://agupubs.onlinelibrary.wiley.com/doi/abs/10.1029/JC093iC09p10749, doi:10.1029/JC093iC09p10749.

Osborne, J.M., Bernabeu, M.O., Bruna, M., Calderhead, B., Cooper, J., Dalchau, N., Dunn, S.J., Fletcher, A.G., Freeman, R., Groen, D., et al., 2014. Ten simple rules for effective computational research. PLoS Computational Biology 10, e1003506.

Petzold, L.R., 1982. Description of DASSL: a differential/algebraic system solver. Technical Report. Sandia National Labs., Livermore, CA (USA).

Plósz, B.G., Liltved, H., Ratnaweera, H., 2009. Climate change impacts on activated sludge wastewater treatment: a case study from norway. Water Science and Technology 60, 533–541.

Reichert, P., 1994. Aquasim-a tool for simulation and data analysis of aquatic systems. Water Science and Technology 30, 21.

Reichert, P., 1998. Aquasim 2.0-tutorial. Swiss Federal Institute for Environmental Science and Technology (EAWAG): Dübendorf, Switzerland .

Rodríguez-Miranda, E., Acién, F.G., Guzmán, J.L., Berenguel, M., Visioli, A., 2021. A new model to analyze the temperature effect on the microalgae performance at large scale raceway reactors. Biotechnology and Bioengineering 118, 877–889.

Rosén, C., Jeppsson, U., 2006. Aspects on ADM1 Implementation within the BSM2 Framework. Department of Industrial Electrical Engineering and Automation, Lund University, Lund, Sweden .

Rossi, S., Casagli, F., Mantovani, M., Mezzanotte, V., Ficara, E., 2020a. Selection of photosynthesis and respiration models to assess the effect of environmental conditions on mixed microalgae consortia grown on wastewater. Bioresource technology 305, 122995.

Rossi, S., Sforza, E., Pastore, M., Bellucci, M., Casagli, F., Marazzi, F., Ficara, E., 2020b. Photo-respirometry to shed light on microalgae-bacteria consortia—a review. Reviews in Environmental Science and Bio/Technology 19, 43–72.

Rosso, L., Lobry, J., Flandrois, J., 1993. An unexpected correlation between cardinal temperatures of microbial growth highlighted by a new model. Journal of Theoretical Biology 162, 447–463.

Rosso, L., Lobry, J.R., Bajard, S., Flandrois, J.P., 1995. Convenient model to describe the combined effects of temperature and pH on microbial-growth. Applied and Environmental Microbiology 61, 610–616.

Sánchez-Zurano, A., Rodríguez-Miranda, E., Guzmán, J.L., Acién-Fernández, F.G., Fernández-Sevilla, J.M., Molina Grima, E., 2021. Abaco: A new model of microalgae-bacteria consortia for biological treatment of wastewaters. Applied Sciences 11, 998.

Sedory, P.E., Stenstrom, M., 1995. Dynamic prediction of wastewater aeration basin temperature. Journal of Environmental Engineering 121, 609–618.

Shampine, L.F., Reichelt, M.W., Kierzenka, J.A., 1999. Solving index-1 daes in matlab and simulink. SIAM review 41, 538–552.

Solimeno, A., Gómez-Serrano, C., Acién, F.G., 2019. Bio_algae 2: improved model of microalgae and bacteria consortia for wastewater treatment. Environmental Science and Pollution Research 26, 25855–25868.

Van Fan, Y., Chin, H.H., Klemeš, J.J., Varbanov, P.S., Liu, X., 2020. Optimisation and process design tools for cleaner production. Journal of Cleaner Production 247, 119181.

Van Fan, Y., Varbanov, P.S., Klemeš, J.J., Nemet, A., 2018. Process efficiency optimisation and integration for cleaner production.

Wágner, D.S., Valverde-Perez, B., Sæbø, M., de la Sotilla, M.B., Van Wagenen, J., Smets, B.F., Plosz, B.G., 2016. Towards a consensus-based biokinetic model for green microalgae–the asm-a. Water research 103, 485–499.

Wolf, G., Picioreanu, C., van Loosdrecht, M.C., 2007. Kinetic modeling of phototrophic biofilms: the phobia model. Biotechnology and bioengineering 97, 1064–1079.

Yong, J.Y., Klemeš, J.J., Varbanov, P.S., Huisingh, D., 2016. Cleaner energy for cleaner production: modelling, simulation, optimisation and waste management. Journal of Cleaner Production 111, 1–16.

Yu, Q., Feng, L., Zhen, X., 2021. Effects of organic loading rate and temperature fluctuation on the microbial community and performance of anaerobic digestion of food waste. Environmental Science and Pollution Research 28, 13176–13187.

Zouboulis, A., Tolkou, A., 2015. Effect of climate change in wastewater treatment plants: reviewing the problems and solutions, in: Managing water resources under climate uncertainty. Springer, pp. 197–220.

Simulating biotechnological processes affected by meteorology: application to algae-bacteria systems

Francesca Casagli[a], Olivier Bernard[a,b*]

[c]*BIOCORE, INRIA, Université côte d'Azur, BP 93, 06902 Sophia-Antipolis Cedex, France.*
[d]*LOV, Sorbonne University, CNRS, UMR 7093, Station Zoologique, BP 28, 06234 Villefrance-sur-mer, France.*

SUPPORTING INFORMATION

Appendix A. Experimental protocol (Narbonne case study)

Details on the experimental protocol can be found in Casagli et al. (2021b). Briefly, the HRABP was realized in concrete and placed on the ground over a base of concrete (thickness 0.2 m). It was mixed with a paddle wheel, operated to obtain a water linear velocity of 0.2 m s^{-1}, and an additional mixing pump that was located at the opposite side of the paddle wheel (operated at the flow rate of 182 m^3 d^{-1}). T The outflow was implemented by gravity overflow, resulting in a variable liquid depth (min 0.257 m, max 0.368 m), measured with an ultrasonic distance sensor (Siemens, SITRANS Probe 7ML5221-1BB11). The HRABP was also equipped with online dissolved oxygen (METTLER TOLEDO, InPro 6850i), temperature and pH

*Corresponding author
Email address: olivier.bernard@inria.fr (Olivier Bernard[a,b*])

(METTLER TOLEDO, InPro4260(i)/SG/425) probes. The incident light (expressed as Photosynthetically Active Radiation, PAR) was continuously measured at the reactor surface, using a PAR meter (SKYE Instruments, PAR 2625). All the online measurements were collected every five minutes, using the dedicated SILEX-LBE acquisition system (INRAE-LBE, France).

Appendix B. Recall of modelling principes

Appendix B.1. Modelling the influence of pH

There are different kinetics models representing the influence of pH. The most used being probably the one proposed by Rosso et al. (1995), i.e. the Cardinal pH Model (CPM).The CPM is zero for $pH \notin [pH_{min},\ pH_{max}]$, where pH_{min} and pH_{max} are the minimum and the maximum pH thresholds respectively. For $pH \in [pH_{min},\ pH_{max}]$ the pH effect is described by f_{pH}, where pH_{opt} is the pH value at which f_{pH} is maximum:

$$f_{pH} = \frac{(pH - pH_{max}) \cdot (pH - pH_{min})}{(pH - pH_{min}) \cdot (pH - pH_{max}) - (pH - pH_{opt})^2} \tag{B.1}$$

Appendix B.2. Modelling the influence of temperature

The temperature in outdoor open bioreactors fluctuates within large ranges according to daily and seasonal dynamics. The fluctuations are of higher amplitudes for the processes with lower depths. The temperature dependence is often modelled through the Cardinal Temperature Model with Inflection (CTMI), that requires three parameters, i.e. the cardinal temperatures: T_{max}, T_{min} and T_{opt} (Rosso et al., 1993). The CTMI is zero for

$T_R \notin [T_{min},\ T_{max}]$, where T_{min} is the temperature below which no growth occurs and T_{max} is the maximum temperature above which there is no more growth. For $T_R \in [T_{min},\ T_{max}]$ the temperature effect is given by the function $f_{T,1}$. T_{opt} being the temperature at which $f_{T,1}$ is maximum:

$$f_{T,1} = \frac{(T - T_{max}) \cdot (T - T_{min})^2}{(T_{opt} - T_{min}) \cdot [(T_{opt} - T_{min}) \cdot (T - T_{opt}) - (T_{opt} - T_{max}) \cdot (T_{opt} + T_{min} - 2T)]} \tag{B.2}$$

Appendix B.3. Modelling the influence of nutrients

The combined effect of nutrients is classically represented by the multiplication of two terms, each one representing an individual effect, or by a Liebig's minimum law (De Baar, 1994), stating that growth is triggered by the most limiting element. There are also more complicated way of integrating the nonlinear interactions between two limiting nutrients (Bertolazzi, 2005; Bougaran et al., 2010).

Appendix B.4. Modelling the influence of light

An additional aspect arises for microalgae, whose dynamics depends on light distribution in the water column. Light intensity decreases along the culture, due to its absorption and scattering. Light is a crucial factor for algal growth, driving a large fraction of the energy and carbon fluxes in the system. The simple Lambert-Beer law is often chosen to represent light extinction in the system:

$$I(I_0, z) = I_0 e^{-\epsilon(\xi) z} \tag{B.3}$$

where the light extinction rate $\epsilon(\xi)$ is proportional to the biomass of algae in most of the model, but can account for the background turbidity (Martínez et al., 2018), possibly including other particulate compounds. It can even be a nonlinear function of the algal biomass (Morel, 1988).

There are several ways of representing this effect (Béchet et al., 2013), depending on if only the average light intensity or the average growth rate are considered.

Appendix C. Summary of the ALBA model development choices

Here, we recall the main choices made in the construction of the model. We refer the reader to Casagli et al. (2021b,a) for more details. Reaction stoichiometry, rates and nomenclature are in line with the IWA modelling works, i.e. Activated Sludge Models (ASMs) and Anaerobic Digestion Model n°1 (ADM1), ((Batstone et al., 2002), (Henze et al., 2000b)).

The biokinetic rates are based on the Liebig's minimum law (De Baar, 1994) for limiting substrates (carbon, nitrogen and phosphorus), meaning that the most limiting nutrient drives the overall kinetics. The general expression describing the structure of bioprocess rates is:

$$\rho_j = \mu_{max_j} \cdot f_T \cdot f_{pH} \cdot \frac{K_n}{K_n + S_n} \cdot \min_i \left(\frac{S_i}{S_i + K_{S_i}} \right) \cdot X_{BM_i} \tag{C.1}$$

Where μ_{max_j} is the maximum specific growth rate [d^{-1}] related to the process ρ_j; f_T, f_{pH} and f_I are the functions describing temperature and pH dependence, respectively; K_n is the inhibition constant for the inhibiting

substrate S_n, K_{S_i} is the half-saturation constant for the limiting substrate S_i and $X_{BM,i}$ is the biomass associated to the process ρ_j.

The photosynthesis response to irradiance is described computing the average algal growth rate for a given incident light and liquid depth. It accounts for the light extinction through the Beer-Lambert law (B.3), and for the actual growth rate at a certain depth. The chosen Haldane-type function represents the limiting light in the darkest parts of the reactor and photoinhibition at high irradiance close to the surface (Bernard and Remond, 2012):

$$\mu_{opt}(I(z)) = \mu_{max} \frac{I(z)}{I(z) + \frac{\mu_{max}}{\alpha} \left(\frac{I(z)}{I_{opt}} - 1 \right)^2} \tag{C.2}$$

The average growth rate is the reactor in then computed as follows:

$$\bar{\mu}(I_0, h) = \frac{1}{h} \int_0^h \mu(I(I_0, z)) dz \tag{C.3}$$

The temperature dependence for algae and bacteria growth is modelled through the Cardinal Temperature Model with Inflection (CTMI), see Equation (B.2), (Rossi et al., 2020a).

The Arrhenius function, depending only on one parameter, was chosen for the decay rates:

$$f_{T,2} = \theta^{T-20} \tag{C.4}$$

The pH strongly influences system dynamics, since it directly affects the dissociation of the majority of soluble compounds (S_{IC}, S_{NH}, S_{NO2}, S_{NO3},

S_{PO4}). The influence of pH on algae and bacteria bio-process rates is included through CPM function proposed by (Rosso et al., 1995).

Appendix D. Petersen matrix for the ALBA model

component j → / process i ↓	X_{ALG} gCOD m^{-3}	X_{AOB} gCOD m^{-3}	X_{NOB} gCOD m^{-3}	X_H gCOD m^{-3}	X_S gCOD m^{-3}	X_I gCOD m^{-3}	S_S gCOD m^{-3}	S_I gCOD m^{-3}	S_{IC} gCm^{-3}	S_{ND} gNm^{-3}	S_{NH} gNm^{-3}	S_{NO2} gNm^{-3}	S_{NO3} gNm^{-3}	S_{N2} gNm^{-3}	S_{PO4} gPm^{-3}	S_{O2} gO_2m^{-3}	S_{H2O} gHm^{-3}
Algae																	
1 phototrophic growth on NH_4^+	1								$\alpha_{1,9}$		$\alpha_{1,11}$				$\alpha_{1,15}$	1	$\alpha_{1,17}$
2 phototrophic growth on NO_3^-	1								$\alpha_{2,9}$				$\alpha_{2,13}$		$\alpha_{2,15}$	1	$\alpha_{2,17}$
3 aerobic respiration	-1								$\alpha_{3,9}$		$\alpha_{3,11}$				$\alpha_{3,15}$	-1	$\alpha_{3,17}$
4 Decay	-1				$\alpha_{4,5}$	$\alpha_{4,6}$			$\alpha_{4,9}$		$\alpha_{4,11}$				$\alpha_{4,15}$		
Heterotrophic bacteria																	
5 Aerobic growth on NH_4^+				1			$\alpha_{5,7}$		$\alpha_{5,9}$		$\alpha_{5,11}$				$\alpha_{5,15}$	$\alpha_{5,16}$	
6 Aerobic growth on NO_3^-				1			$\alpha_{6,7}$		$\alpha_{6,9}$				$\alpha_{6,13}$		$\alpha_{6,15}$	$\alpha_{6,16}$	
7 Aerobic respiration				-1					$\alpha_{7,9}$		$\alpha_{7,11}$				$\alpha_{7,15}$	-1	
8 Anoxic growth on NO_3^-				1			$\alpha_{8,7}$		$\alpha_{8,9}$		$\alpha_{8,11}$		$\alpha_{8,13}$	$\alpha_{8,14}$	$\alpha_{8,15}$		
9 Anoxic growth on NO_2^-				1			$\alpha_{9,7}$		$\alpha_{9,9}$		$\alpha_{9,11}$	$\alpha_{9,12}$		$\alpha_{9,14}$	$\alpha_{9,15}$		
10 Anoxic respiration NO_2^- and NO_3^-				-1					$\alpha_{10,9}$		$\alpha_{10,11}$	$\alpha_{10,12}$	$\alpha_{10,13}$	$\alpha_{10,14}$	$\alpha_{10,15}$		
11 Hydrolysis of slowly biodegradable COD					-1		$\alpha_{11,7}$	$\alpha_{11,8}$	$\alpha_{11,9}$		$\alpha_{11,11}$				$\alpha_{11,15}$		
12 Hydrolysis of urea									$\alpha_{12,9}$	-1	1						$\alpha_{12,17}$
13 Decay				-1	$\alpha_{13,5}$	$\alpha_{13,6}$			$\alpha_{13,9}$		$\alpha_{13,11}$				$\alpha_{13,15}$		
Ammonium Oxydising Bacteria																	
14 Aerobic growth on NH_4^+		1							$\alpha_{14,9}$		$\alpha_{14,11}$	$\alpha_{14,12}$			$\alpha_{14,15}$	$\alpha_{14,16}$	
15 Aerobic respiration		-1							$\alpha_{15,9}$		$\alpha_{15,11}$				$\alpha_{15,15}$	$\alpha_{15,16}$	
16 Decay		-1			$\alpha_{16,5}$	$\alpha_{16,6}$			$\alpha_{16,9}$		$\alpha_{16,11}$				$\alpha_{16,15}$		
Nitrite Oxydising Bacteria																	
17 Aerobic growth on NO_2^-			1						$\alpha_{17,9}$		$\alpha_{17,11}$	$\alpha_{17,12}$	$\alpha_{17,13}$		$\alpha_{17,15}$	$\alpha_{17,16}$	
18 Aerobic respiration			-1						$\alpha_{18,9}$		$\alpha_{18,11}$				$\alpha_{18,15}$	$\alpha_{18,16}$	
19 Decay			-1		$\alpha_{19,5}$	$\alpha_{19,6}$			$\alpha_{19,9}$		$\alpha_{19,11}$				$\alpha_{19,15}$		

Appendix E. Comparison between the fully predictive ALBA model and simulations with measured temperature

Appendix E.1. Narbonne case study

Figures E.1, E.2 and E.3 show the graphs already reported in Section 4, superimposing the simulation results obtained using the measured temperature.

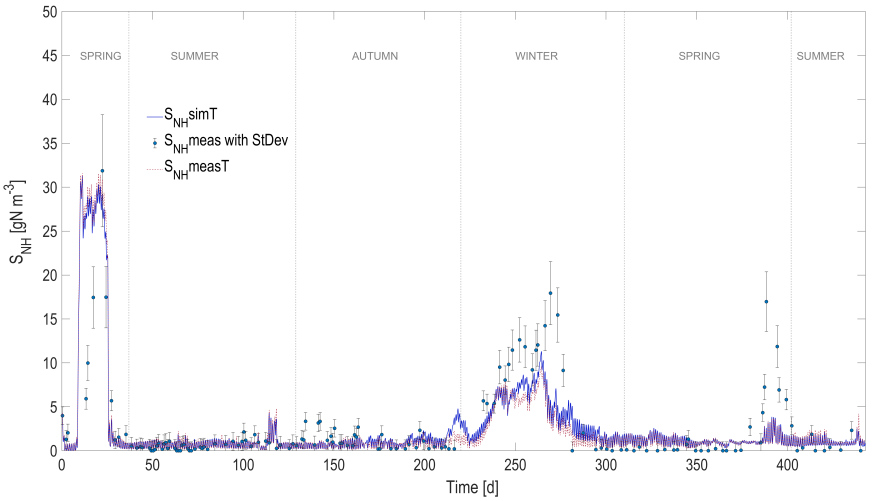

a)

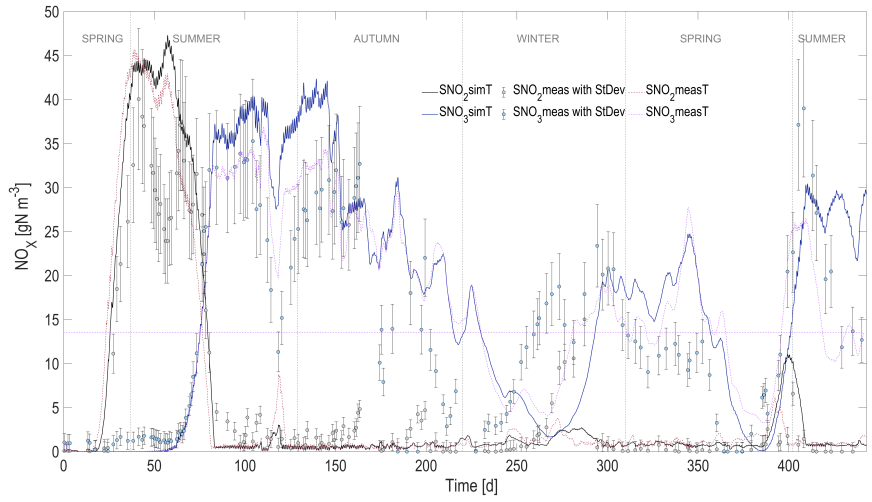

b)

Figure E.1: ALBA fully predictive model validation over one year. Experimental measurements (and their Standard Deviation), model predictions with simulated temperature and model predictions with measured temperature: a) ammoniacal nitrogen; b) nitrite and nitrate.

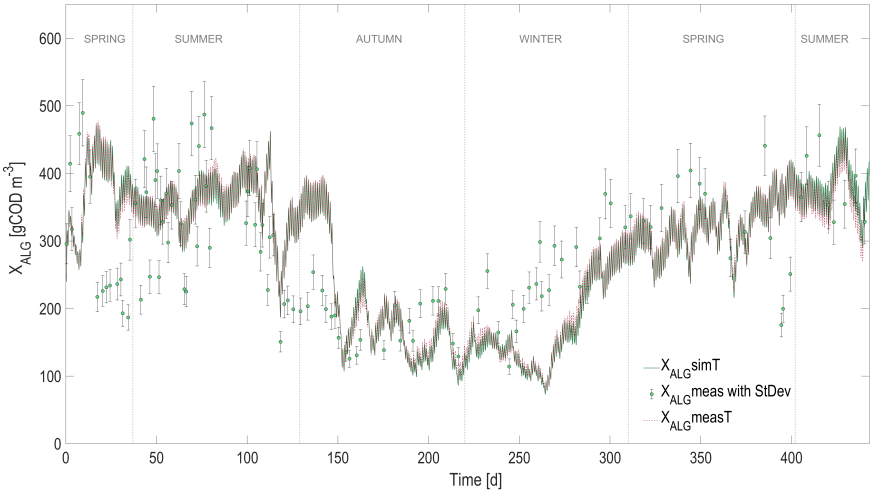

c)

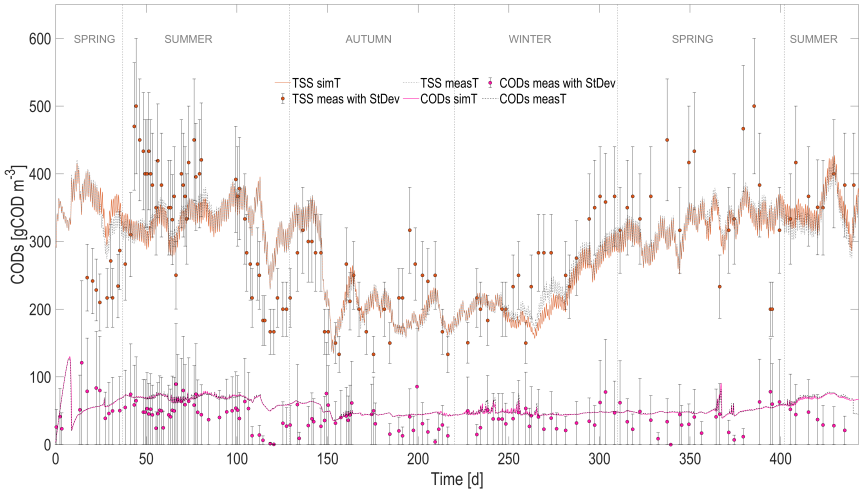

d)

Figure E.2: ALBA fully predictive model validation over one year. Experimental measurements (and standard deviation), model predictions with simulated temperature and model predictions with measured temperature: c) algal biomass; d) Total Suspended Solids and soluble COD

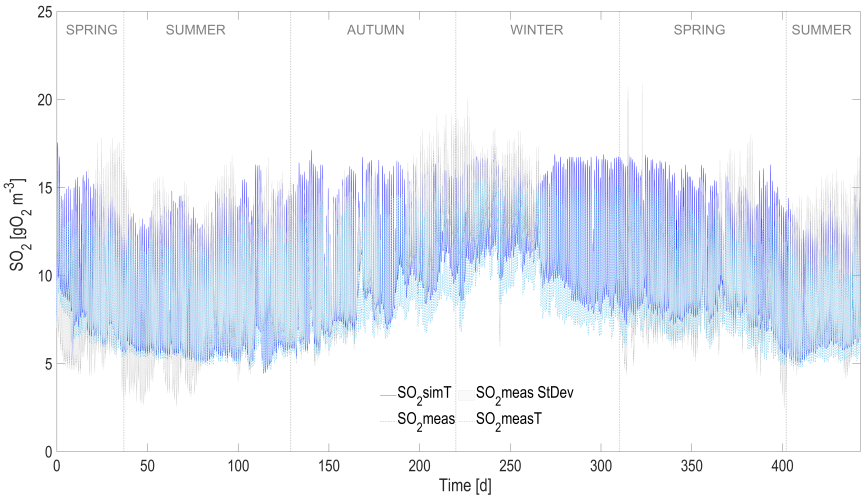

e)

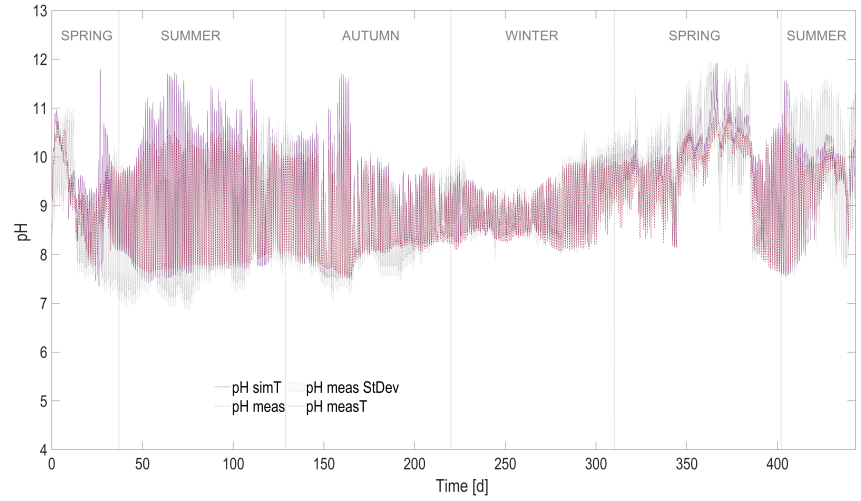

f)

Figure E.3: ALBA fully predictive model validation over one year. Experimental measurements (and their Standard Deviation), model predictions with simulated temperature and model predictions with measured temperature: e) dissolved oxygen; f) pH.

Appendix F. Milan case study

In figures F.5, F.6, F.7 and F.8 the validation results of the fully predictive ALBA model, for another experimental application, are reported. The fully predictive model was validated on experimental data from a pilot-scale HRABP ($1m^3$) located in the northern part of Italy, treating the liquid fraction of piggery digestate. The reactor configuration was different compared to the one located in Narbonne, as shown in Figure F.4, so the heat transfer model was adapted, removing the heat flux with the ground (conduction term) and adding the conductive /convective term between the liquid, the material of the pond and the air. More details concerning this experimentation can be found in A.Pizzera et al. (2019); Casagli et al. (2021a).

The model resulted to be very accurate in both the predictions of the pond temperature and the main measured variables, as ammoniacal nitrogen, nitrite, nitrate, algal biomass and oxygen.

In figure F.6, F.7 and F.8, the dots represent the measurements with their standard deviation, the continuous lines are the simulation results, while the shaded areas are the error bounds for the model predictions, computed on the first version of the ALBA model (i.e.where the measured temperature was used). The continuous line falls always in the shaded areas and it follows very well the trend of the experimental data, confirming indirectly the accuracy of the heat transfer model, applied also to this case study.

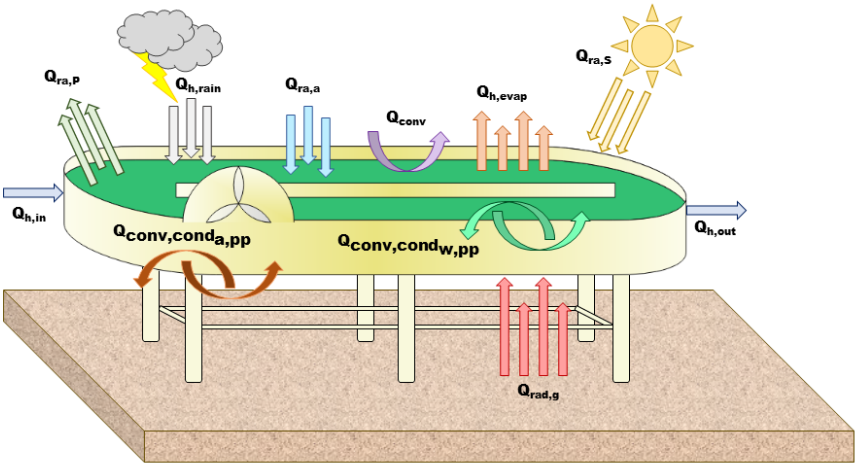

Figure F.4: Configuration of the HRABP located in Milan

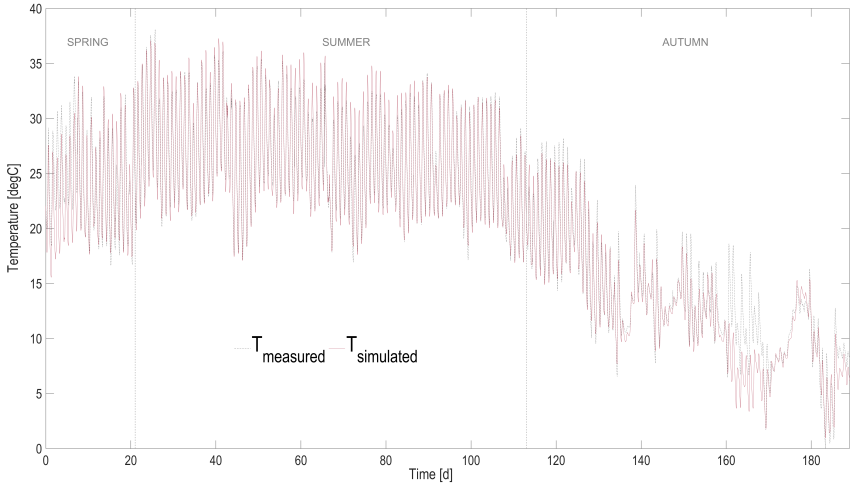

a)

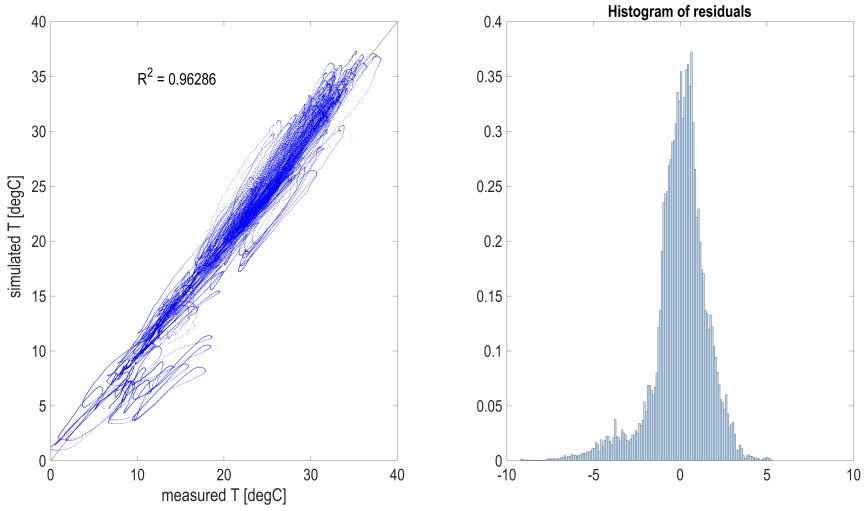

b)

Figure F.5: Heat transfer model validation over six months experimental measurements (54410 measured temperature values)

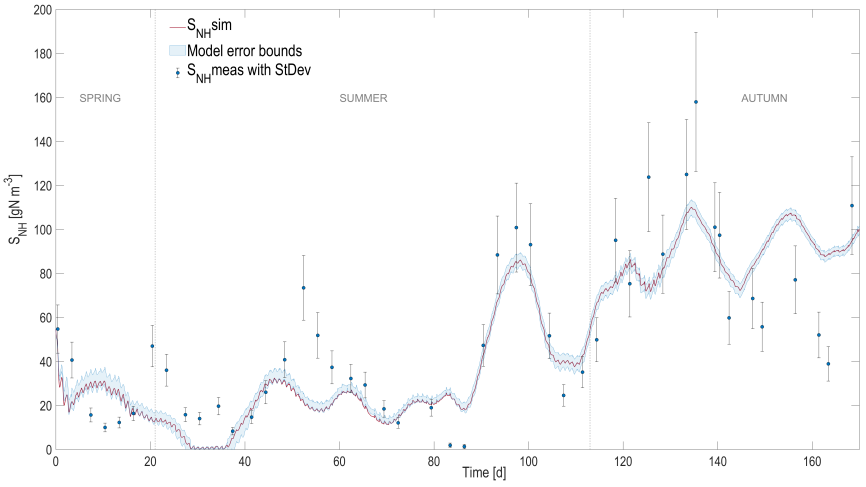

a)

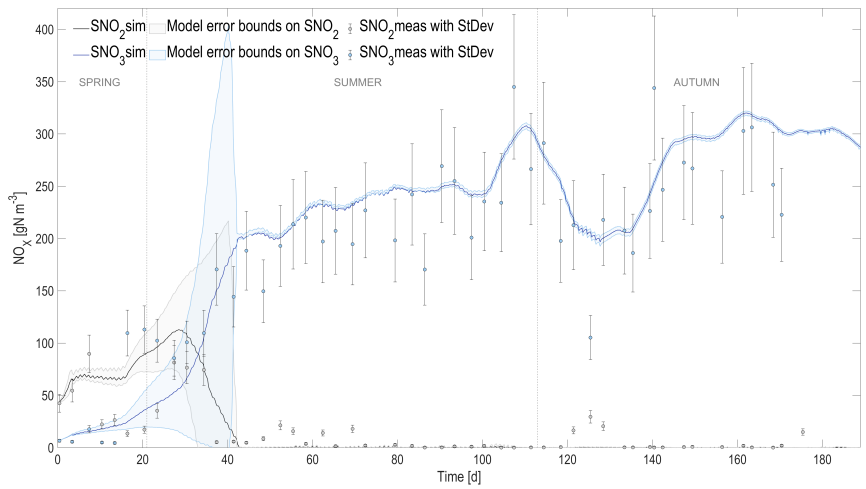

b)

Figure F.6: Full prediction capability of the coupled thermal-biology ALBA model. Comparison between predictions with simulated temperature (together with model error bounds) and measurements for: a) ammoniacal nitrogen; b) nitrite and nitrate.

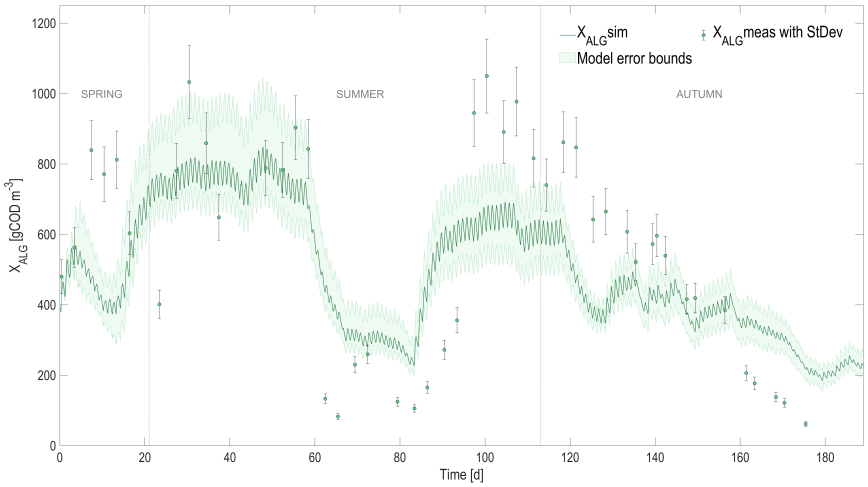

c)

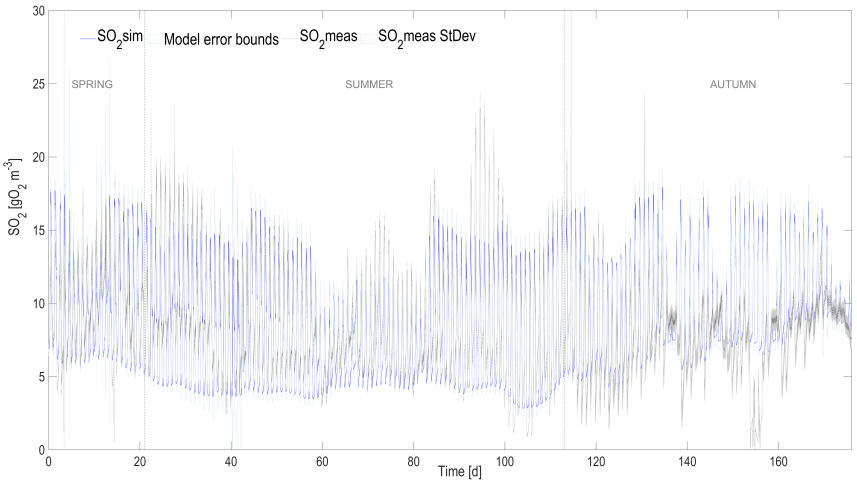

d)

Figure F.7: Full prediction capability of the coupled thermal-biology ALBA model. Comparison between predictions with simulated temperature (together with model error bounds) and measurements for: c) algal biomass; d) dissolved oxygen.

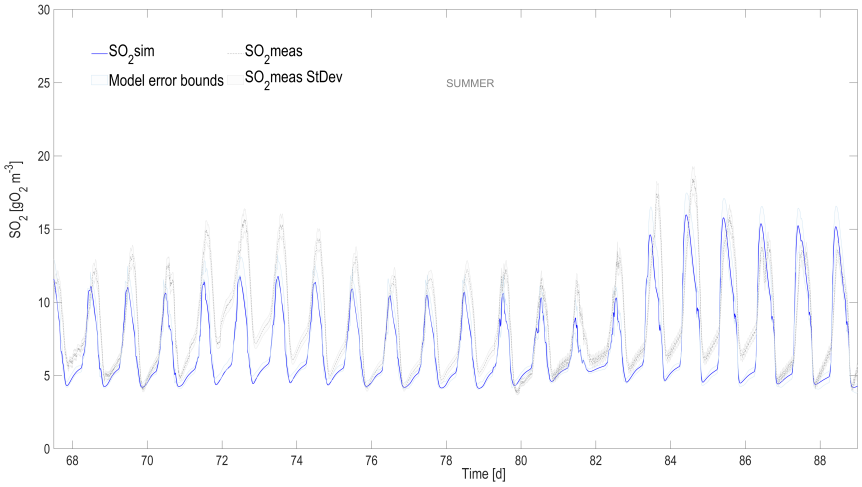

e)

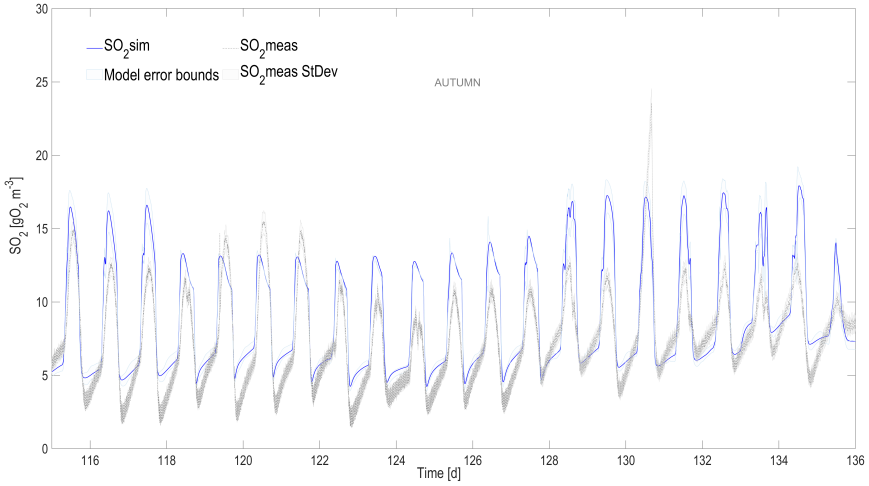

f)

Figure F.8: Full prediction capability of the coupled thermal-biology ALBA model. Comparison between predictions with simulated temperature (together with model error bounds) and measurements for: e) dissolved oxygen: focus on summer season; f) dissolved oxygen: focus on autumn season.

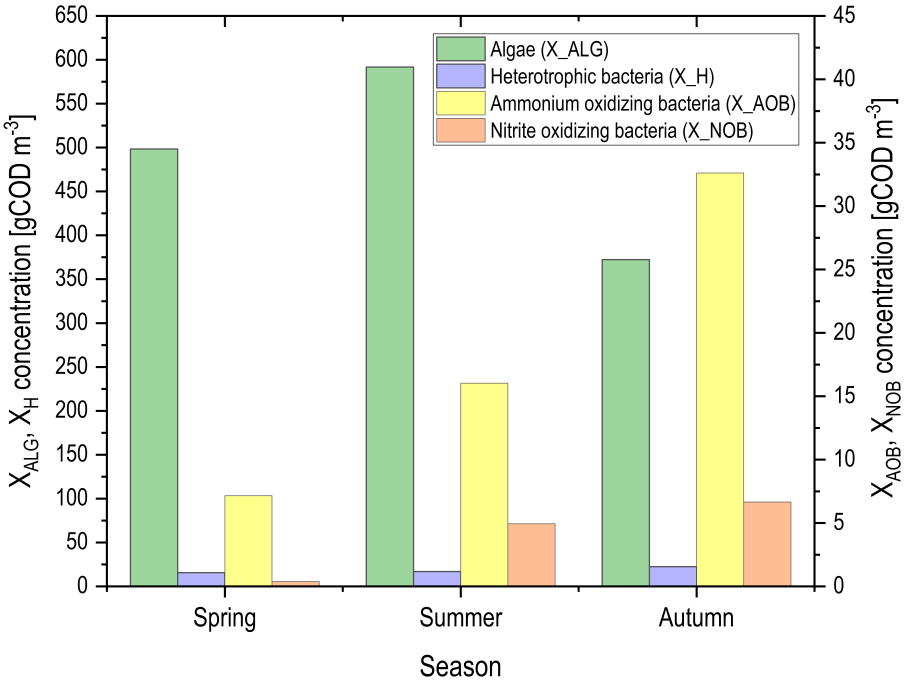

Figure F.9: Average composition of the microbial population according to seasons, as estimated by the fully predictive model. Right axis: algae (X_{ALG}) and heterotrophic bacteria (X_H) concentration; left axis: nitrifying bacteria (X_{AOB} and X_{NOB}) concentration.

Appendix G. Temperature impact on equilibrium constants

On the wave of the work performed from the ADM1 task group, the temperature impact on the equilibrium coefficients ($K_{a,T}$, $[molL^{-1}]$) can be taken into account by using the van't Hoff equation:

$$ln\frac{K_{a,T}}{K_{a,T_{ref}}} = \frac{\Delta H}{R}\left(\frac{1}{T_{ref}} - \frac{1}{T+273.15}\right) \tag{G.1}$$

where T_{ref} is the standard temperature (i.e. 298.15 K) for which the value of the equilibrium coefficient ($K_{a,T_{ref}}$, $[molL^{-1}]$) is known. R is the gas law constant $[JK^{-1}mol^{-1}]$ and ΔH is the heat of reaction at standard temperature and pressure $[Jmol^{-1}]$.

Appendix H. Total alkalinity and inorganic carbon concentration: effect of wrong temperature predictions in HRABPs

In order to show the temperature effect on key variables as the inorganic carbon (S_{IC}) and the total alkalinity (TA), additional simulations were run. Specifically, the predictions obtained with the fully predictive ALBA model were compared with the results obtained using the measured temperature increased and decreased of 5 degC, respectively. The results of the comparison are reported in figure H.10. Concerning the total alkalinity, the average absolute/relative error computed when increasing and decreasing the temperature, is 26.74% and 16.65% respectively, while the maximum one is 140.59% and 144.04% respectively. Focusing on the total inorganic carbon, the average and maximum absolute/relative error, when increasing the temperature, are 50.84% and 295.39% respectively. When decreasing the temperature, the

average and maximum absolute/relative error are 32.64% and 201.65% respectively.

It is therefore shown how much the total alkalinity and the inorganic carbon trends are affected by a relatively small temperature variation ($\pm 5 deg C$). In addition, these two variables are strictly linked to: i) photoautotrophic and autotrophic growth (algae and nitrifiers); ii) CO_2 stripping and iii) suitable conditions for N_2O production (if occuring inorganic carbon limitation). Therefore, an accurate temperature prediction in the reactor is required.

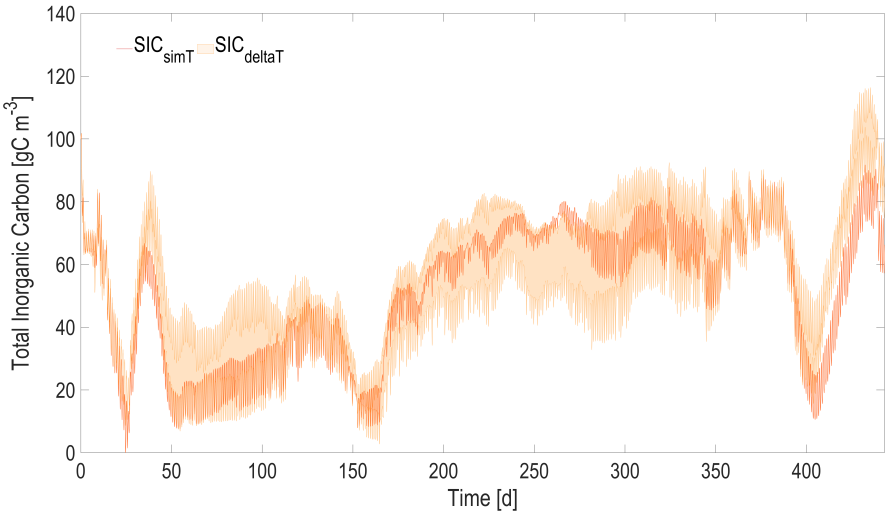

a)

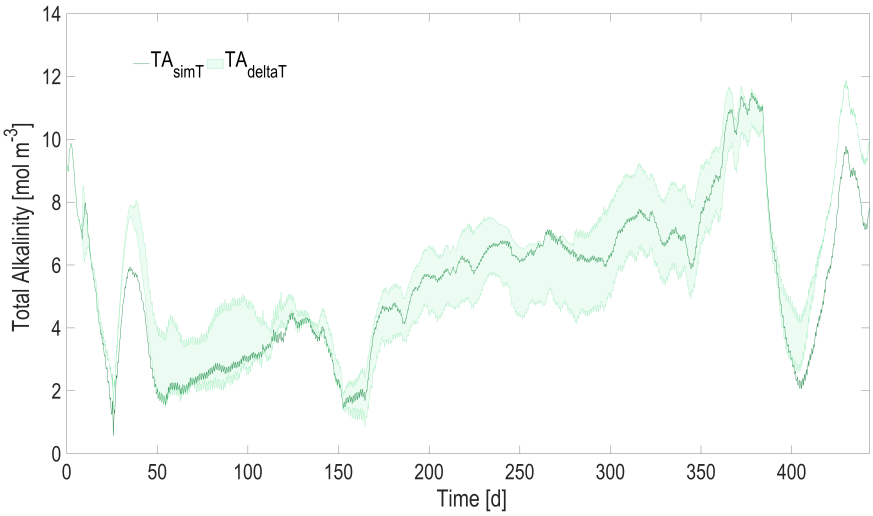

b)

Figure H.10: Predicted values for total alkalinity (a) and inorganic carbon (b): the continuous lines represent the simulation results obtained using the fully predictive model; the shaded areas represent the total alkalinity and inorganic carbon range of variation for temperature $\pm 5^{\circ}$ C.

Appendix I. Parameters used for the extended version of the heat transfer model

The parameters required for running the heat transfer model are reported in the following Table I.3.

Table I.3: Parameter values for the heat transfer model.

Symbol	Definition	Unit	Value
Water parameters			
ρ_w	Water density	kg m^{-3}	998
Cp_w	Water heat capacity	J kg^{-1} K^{-1}	$4.18 \cdot 10^3$
L_w	Water latent heat	J kg^{-1}	$2.45 \cdot 10^6$
ϵ_w	Water emissivity	-	0.97
M_w	Water molecular weight	kg m^{-3}	0.018
Soil parameters			
k_s	Soil thermal conductivity	W m^{-1} K^{-1}	2
Cp_s	Soil specific heat capacity	J kg^{-1} K^{-1}	$1.25 \cdot 10^3$
ρ_s	Soil density	kg m^{-3}	$1.9 \cdot 10^3$
$l_{s,ref}$	Depth at which the soil temperature is constant over the year	m	5
$T_{s,ref}$	Soil temperature at $l_{s,ref}$	°C	10
Air parameters			
ϵ_a	Air emissivity	-	0.8
v_a	Air kinematic viscosity	m^2 s^{-1}	$1.5 \cdot 10^{-5}$
λ_a	Air thermal conductivity	W m^{-1} K^{-1}	$2.6 \cdot 10^{-2}$
Pr_a	Air Prandtl number	-	0.7
ρ_a	Air density	kg m^{-3}	1.2
α_a	Air thermal diffusivity	m^2 s^{-1}	$2.2 \cdot 10^{-5}$
$D_{w,a}$	Mass diffusion coefficient of water vapor in air	m^2 s^{-1}	$2.4 \cdot 10^{-5}$
Pond parameters			
V	Pond volume	m^3	variable
S	Pond surface	m^2	56
L	Pond length	m	15
z	Wind velocity height	m	0.5
z_0	Wind sensor height	m	2.6
q_i	Inflow rate	m^3 s^{-1}	0
f_a	Algal absorption fraction	%	2.5
α	Power law exponent	-	0.29
Concrete parameters			
s_{co}	concrete thickness	m	0.3
ρ_{co}	concrete density	Kg m^3	2500
Cp_{co}	concrete heat capacity	J Kg^{-1} K^{-1}	$1 \cdot 10^3$
$h_{co,w}$	Conductive-convective term (water on concrete)	W m^{-2} K^{-1}	8.5[a]
Universal constants			
σ	Stephan-Boltzmann constant	W m^{-2} K^{-4}	$5.67 \cdot 10^{-8}$
R	Ideal gas constant	Pa m^3 mol^{-1} K^{-1}	8.314

[a] computed considering: i) concrete thermal conductivity 2.6 W m^{-1} K^{-1}; ii) water thermal convection coefficient 10^3 W m^{-2} K^{-1}

Appendix J. Extending the pH submodel in the presence of VFA

.

Table J.4: Chemical sub-model extension when volatile fatty acids are present in the medium.
HAc : CH_3COOH, Ac^- : CH_3COO^- HBr : $CH_3CH_2CH_2COOH$, Br^- : $CH_3CH_2CH_2COO^-$ HPr : CH_3CH_2COOH, Pr^- : $CH_3CH_2COO^-$, HVa : $CH_3CH_2CH_2CH_2COOH$, Pr^- : $CH_3CH_2CH_2CH_2COO^-$

Description	Expression $[molm^{-3}]$	K_A [M]
	Acetic acid	
1) Mass balance	$\frac{S_{Ac}}{60.05 \cdot 1.07} - HAc - Ac^- = 0$	
2) Dissociation		
$HAC \rightleftharpoons AC^- + H^+$	$HAc - \frac{\frac{S_{Ac}}{60.05 \cdot 1.07}}{1+\frac{KA_{Ac}10^3}{H^+}} = 0$	$K_{A,Ac} = 1.74E{-}5$
	Butyric acid	
3) Mass balance	$\frac{S_{Bu}}{88.11 \cdot 1.82} - HBu - Bu^- = 0$	
4) Dissociation		
$HBu \rightleftharpoons Bu^- + H^+$	$HBu - \frac{\frac{S_{Bu}}{88.11 \cdot 1.82}}{1+\frac{KA_{Bu}10^3}{H^+}} = 0$	$K_{A,Bu} = 1.51E{-}5$
	Propionic acid	
5) Mass balance	$\frac{S_{Pr}}{74.08 \cdot 1.51} - HPr - Pr^- = 0$	
6) Dissociation		
$HPr \rightleftharpoons Pr^- + H^+$	$HPr - \frac{\frac{S_{Pr}}{74.08 \cdot 1.51}}{1+\frac{KA_{Pr}10^3}{H^+}} = 0$	$K_{A,Pr} = 1.32E{-}5$
	Valeric acid	
7) Mass balance	$\frac{S_{Va}}{102.13 \cdot 2.04} - HVa - Va^- = 0$	
8) Dissociation		
$HVa \rightleftharpoons Va^- + H^+$	$HVa - \frac{\frac{S_{Va}}{102.13 \cdot 2.04}}{1+\frac{KA_{Va}10^3}{H^+}} = 0$	$K_{A,Va} = 9.77E{-}6$
	Hydrogen sulphide	
9) Mass balance	$\frac{S_{H_2S}}{32.07} - H_2S - HS^- - S^{2-} = 0$	
10) Dissociation		
$H_2S \rightleftharpoons HS^- + H^+$	$H_2S - \frac{S_{H_2S}/32.07}{1+\frac{Ka_{H_2S}10^3}{H^+}+\frac{Ka_{H_2S}Ka_{HS^-}10^6}{(H^+)^2}} = 0$	$K_{A,H_2S} = 8.91E{-}8$
11) Dissociation		
$HS^- \rightleftharpoons S^{2-} + H^+$	$HS^- - \frac{S_{H_2S}/32.07}{1+\frac{H^+}{Ka_{H_2S}10^3}+\frac{Ka_{HS^-}10^3}{H^+}} = 0$	$K_{A,HS^-} = 1.29E{-}13$

Appendix K. Solving the pH submodel

.

The way the pH submodel is numerically solved is illustrated for the ALBA model. It consists in determining 15 unknown (NH_3, NH_4^+, NO_2^-, HNO_2, NO_3^-, HNO_3, CO_2, HCO_3^-, CO_3^{2-}, H_3PO_4, $H_2PO_4^-$, HPO_4^{2-}, PO_4^{3-}, OH^- and H^+) from the 5 state variables $S_{PO_4}, S_{NO_2}, S_{NO_3}, S_{NH}$ and S_{IC} supporting the 5 mass balances and the 9 equations for the dissociation, plus the one for the charge balance. To solve this system, the charge balance equation can be rewritten accounting for the dependence of the dissociated fractions from the H^+ ions and from the total amount of compounds.

$$\begin{aligned} H^+ \quad & +NH_4^+(H^+, S_{NH}) + \Delta_{CAT,AN} - OH^-(H^+) \\ & -NO_2^-(H^+, S_{NO_2}) - NO_3^-(H^+, S_{NO_3}) - HCO_3^-(H^+, S_{IC}) \\ & -2CO_3^{2-}(H^+, S_{IC}) - H_2PO_4^-(H^+, S_{PO_4}) \\ & -2HPO_4^{2-}(H^+, S_{PO_4}) - 3PO_4^{3-}(H^+, S_{PO_4}) \qquad = 0 \end{aligned} \tag{K.1}$$

which can be rewritten as

$$H^+ = \Phi_{\mathrm{pH}}(H^+, S_{PO_4}, S_{NO_2}, S_{NO_3}, S_{NH}, S_{IC}) \tag{K.2}$$

The physical root of this equation can be solved by an algebraic solver. Here we prefer to compute the variable $\hat{H}^+$ which is an estimate of H^+. The estimator equation is given by

$$\frac{d\hat{H}^+}{dt} = \hat{K}\left(\Phi_{\mathrm{pH}}(\hat{H}^+, S_{PO_4}, S_{NO_2}, S_{NO_3}, S_{NH}, S_{IC}) - \hat{H}^+\right) \tag{K.3}$$

where $\hat{K}$ is a constant tuning the rate for solving the pH equation. Note that, for each equilibrium, $\hat{H}^+$ automatically satisfies Equation (K.2). At the time scale defined by $\frac{1}{\hat{K}}$, the other state variables can be considered as constant (fast-slow system).